

Paleoceanography and Paleoclimatology

RESEARCH ARTICLE

10.1029/2019PA003836

Key Points:

- We present a new coral proxy system model to facilitate comparison between proxy observations and climate model output
- Analytical and calibration errors, variable growth rates, and age modeling uncertainties all have measurable impacts on interannual variance
- The relative importance of different uncertainties on interannual variance are site dependent

Supporting Information:

- Supporting Information S1

Correspondence to:

A. E. Lawman,
alawman@utexas.edu

Citation:

A. E. Lawman, J. W. Partin, S. G. Dee, C. A. Casadio, P. Di Nezio, & T. M. Quinn (2020). Developing a coral proxy system model to compare coral and climate model estimates of changes in paleo-ENSO variability. *Paleoceanography and Paleoclimatology*, 35, e2019PA003836. <https://doi.org/10.1029/2019PA003836>

Received 16 DEC 2019

Accepted 1 JUN 2020

Accepted article online 16 JUN 2020

Author Contributions:

Conceptualization: J. W. Partin, S. G. Dee, P. Di Nezio

Data curation: A. E. Lawman, J. W. Partin, C. A. Casadio

Formal analysis: A. E. Lawman, J. W. Partin, S. G. Dee, C. A. Casadio, P. Di Nezio

Funding acquisition: J. W. Partin

Methodology: A. E. Lawman, J. W. Partin, S. G. Dee, C. A. Casadio, P. Di Nezio, T. M. Quinn

Software: A. E. Lawman, S. G. Dee, C. A. Casadio




Supervision: J. W. Partin, T. M. Quinn

Validation: A. E. Lawman, J. W. Partin, S. G. Dee, C. A. Casadio, P. Di Nezio, T. M. Quinn

Visualization: A. E. Lawman, C. A. Casadio

(continued)

Developing a Coral Proxy System Model to Compare Coral and Climate Model Estimates of Changes in Paleo-ENSO Variability

A. E. Lawman^{1,2} , J. W. Partin¹ , S. G. Dee³ , C. A. Casadio¹ , P. Di Nezio¹, and T. M. Quinn^{1,2} 

¹Institute for Geophysics, Jackson School of Geosciences, The University of Texas at Austin, Austin, TX, USA,

²Department of Geological Sciences, Jackson School of Geosciences, The University of Texas at Austin, Austin, TX, USA,

³Department of Earth, Environmental and Planetary Sciences, Rice University, Houston, TX, USA

Abstract Coral records of surface-ocean conditions extend our knowledge of interannual El Niño–Southern Oscillation (ENSO) variability into the preinstrumental period. That said, the wide range of natural variability within the climate system as well as multiple sources of uncertainties inherent to the coral archive produce challenges for the paleoclimate community to detect forced changes in ENSO using coral geochemical records. We present a new coral proxy system model (PSM) of intermediate complexity, geared toward the evaluation of changes in interannual variance. Our coral PSM adds additional layers of complexity to previously published transfer functions of sensor models that describe how the archive responds to sea surface temperature (SST) and salinity. We use SST and salinity output from the Community Earth System Model Last Millennium Ensemble 850 control to model coral oxygen isotopic ratios and SST derived from Sr/Ca. We present a detailed analysis of our PSM using climate model output for sites in the central and southwest Pacific before extending the analyses to span the broader tropical Pacific. We demonstrate how variable growth rates, analytical and calibration errors, and age model assumptions systematically impact estimates of interannual variance and show that the relative magnitude of the change in interannual variance is location dependent. Importantly, however, we find that even with the added uncertainties in our PSM, corals from many circum-Pacific locations are broadly able to capture decadal and longer (decadal+) changes in ENSO variability. Our code is publicly available on GitHub to facilitate future comparisons between model output and coral proxy data.

Plain Language Summary Climate scientists use the chemistry of coral skeletons to study past tropical climate conditions. The elemental ratio of strontium to calcium (Sr/Ca) and the oxygen isotopic composition ($\delta^{18}\text{O}$) in the coral skeleton are used to reconstruct past sea surface temperature and salinity. Coral Sr/Ca varies in response to changes in sea surface temperature, whereas coral $\delta^{18}\text{O}$ records both changes in temperature and salinity. Individual corals provide tens to hundreds of years of climate information from the tropical oceans. They are well-suited for studying variability related to the El Niño–Southern Oscillation (ENSO), a climate phenomenon that impacts global temperature and rainfall patterns every few years. We rely on both climate proxy data and simulations from global climate models to study changes in ENSO variability in the past. Nevertheless, it is difficult to directly compare proxy data with climate model output due to the imperfect nature of how the climate signal is recorded in the coral skeleton. Proxy system models are a tool designed to help bridge the gap between climate information recorded in corals and climate model output. In this study, we develop a coral proxy system model to demonstrate how different processes impact a coral's ability to record changes in ENSO variability.

1. Introduction

Geochemical records from massive corals provide decades to centuries of subannually resolved proxy climate data from the tropical oceans (Fairbanks et al., 1997; Gagan et al., 2000; Grottoli & Eakin, 2007; Lough, 2010). The ratio of strontium to calcium (Sr/Ca) and the oxygen isotopic composition ($\delta^{18}\text{O}$) of coral skeletal material are established climate proxies (Corrège, 2006; DeLong et al., 2013; Fairbanks et al., 1997; Lough, 2010). Sea surface temperature (SST) exerts the dominant climate control on coral Sr/Ca (Beck et al., 1992; Smith et al., 1979; Weber, 1973), whereas coral $\delta^{18}\text{O}$ is jointly influenced by SST and the

Writing - original draft: A. E. Lawman

Writing - review & editing: A. E. Lawman, J. W. Partin, S. G. Dee, C. A. Casadio, P. Di Nezio, T. M. Quinn

oxygen isotopic composition of seawater ($\delta^{18}\text{O}_{\text{sw}}$) (Gagan et al., 1998; Ren et al., 2003; Weber & Woodhead, 1972), the latter of which is impacted by similar processes as sea surface salinity (e.g., rainfall, evaporation, advection of different water masses, and freshwater runoff) (LeGrande & Schmidt, 2006). One of the major climate applications of geochemical records from tropical Pacific corals is to provide insight about El Niño–Southern Oscillation (ENSO) variability during preinstrumental times.

ENSO is the leading mode of interannual climate variability and has global impacts on temperature and precipitation patterns (Bjerknes, 1969; Ropelewski & Halpert, 1987). SST anomalies (SSTA) averaged across the Niño 3.4 region in the central equatorial Pacific (5°N to 5°S, 120–170°W) are canonically used to determine the occurrence of ENSO events (Trenberth, 1997). Observed SSTA from the Niño 3.4 region shows an increase in the magnitude and frequency of extreme ENSO events over the last few decades (Trenberth & Hoar, 1996; Wang et al., 2019). That said, instrumental observations are of insufficient length (Deser et al., 2010; Fairbanks et al., 1997) to characterize the full range of natural variability in ENSO (Wittenberg, 2009). Furthermore, tropical climate variability is a major source of uncertainty in climate model simulations that project how the Earth will respond to increasing greenhouse gas emissions (Chung et al., 2019; Collins et al., 2013). Different model simulations of future changes in ENSO differ widely in their response to the external forcing of increasing greenhouse gas emissions, as well as in their simulated range of natural (unforced) variability within the climate system (Bellenger et al., 2014; Cai et al., 2014, 2015; Collins et al., 2010; DiNezio et al., 2013). Uncertainties about ENSO projections for the future are a motivation to study ENSO under past climate conditions when the Earth experienced different background conditions. Coral-based climate records that overlap with, and extend beyond, the instrumental period provide important tests of climate model simulations of ENSO (Cobb et al., 2013; Emile-Geay et al., 2016; Gagan et al., 2000; Schmidt et al., 2014).

There are, however, several sources of uncertainty that impact our ability to understand past changes in ENSO variability. These sources of uncertainty include those due to the climate system as well as those from the coral archive. ENSO behavior can vary in the absence of forcings external to the climate system (Deser et al., 2012; Wittenberg, 2009), making it difficult to separate internally versus externally driven changes in variability from short coral records. Clear links between the climate variability experienced at an individual reef site and ENSO must be established through observational study. Lastly, the coral archive itself impacts how a climate signal is recorded. Sources of climate and coral-related uncertainties that impact our ability to characterize past changes in ENSO variability include, but are not limited to the following:

1. the fidelity of a point-source location to capture regional changes in ENSO variability;
2. the range of natural variability within the climate system;
3. the ability of coral Sr/Ca and $\delta^{18}\text{O}$ to record ocean-climate variables;
4. uncertainties in the coral archive that may obscure the climate signal of interest (e.g., variable growth rates); and
5. proxy observation uncertainties (e.g., analytical, calibration, dating, and age model errors)

A proxy system model (PSM) addresses Points 3–5 of the uncertainties listed above, and serves as an important bridge between proxy data and observations or model output (and see Evans et al., 2013; Dee et al., 2015 for a review). PSMs mathematically model how different processes impact a climate signal that emerges from the proxy data. Typically, paleoclimate proxy data is used to reconstruct a climate variable (e.g., SST) using empirically determined calibration equations (Corrège, 2006). Conversely, forward modeling using a PSM broadcasts observations or climate model output into pseudoproxy time series, providing a forward estimate of the proxy signal (Dee et al., 2015; Evans et al., 2013). Previous coral proxy system modeling work developed a transfer function of the sensor model to forward model pseudocoral $\delta^{18}\text{O}$ as a linear combination of SST and sea surface salinity (SSS) (Brown et al., 2008; Thompson et al., 2011):

$$\delta^{18}\text{O}_{\text{pseudocoral}} = a_1 \text{SST} + a_2 \text{SSS}$$

(from Thompson et al., 2011)

The coefficient a_1 is based on the inverse SST dependence that arises from thermodynamic fractionation (Epstein et al., 1953), and the coefficient a_2 is based on observed $\delta^{18}\text{O}_{\text{sw}}$ –SSS relationships (LeGrande & Schmidt, 2006); (see section 2.3.1). Coral PSMs have been employed in previous work to compare a suite

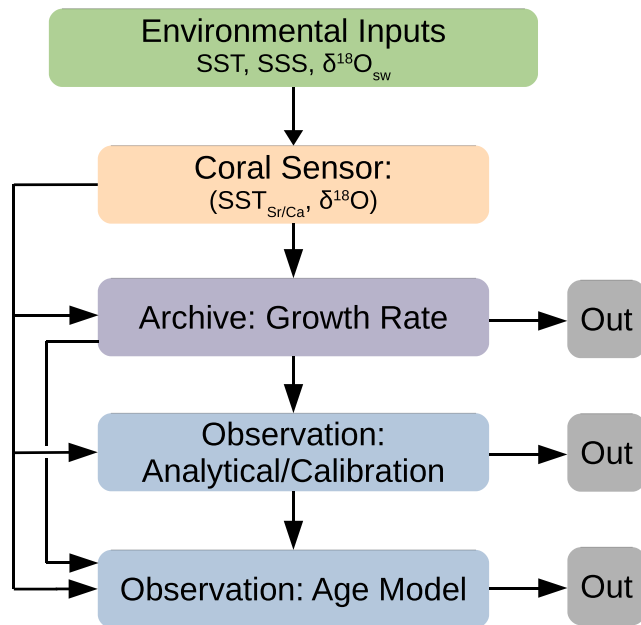


Figure 1. Coral proxy system model (PSM) schematic. The sea surface temperature (SST), sea surface salinity (SSS), or the oxygen isotopic composition of sea water ($\delta^{18}\text{O}_{\text{sw}}$) environmental inputs (green box) can come from instrumental observations, climate model output, or reanalysis data (Dee et al., 2015; Evans et al., 2013). Here and in all subsequent figures, $\text{SST}_{\text{Sr/Ca}}$ refers to SST derived from coral Sr/Ca. The coral $\delta^{18}\text{O}$ sensor model (Thompson et al., 2011) accounts for sensitivity to SST and $\delta^{18}\text{O}_{\text{sw}}$ (SSS). The growth rate archive model (purple box) describes how an environmental signal may be emplaced or transformed in the coral archive due to variable growth rates. The coral observation models (blue boxes) include the combined effect of analytical and calibration errors, as well as age model uncertainties that arise from transforming the coral geochemical from the depth to the time domain. Arrows show possible permutations of the archive and observation submodels to yield pseudocoral output perturbed by the coral PSM (gray boxes). The full coral PSM refers to consecutively perturbing the environmental inputs with the variable growth rate, analytical and calibration, and age model algorithms.

of coral $\delta^{18}\text{O}$ records (Ault et al., 2009) with pseudocorals generated from instrumental observations and climate model simulations for the twentieth century (Thompson et al., 2011). Coral PSMs have also been used to quantify uncertainties in climate signal interpretation (Dee et al., 2015), including errors in coral-based ENSO amplitude (Russon et al., 2015) or ENSO variability estimates (Stevenson et al., 2013).

In this study, we add additional layers of complexity to these previously published transfer functions that describe how the coral archive responds to SST and salinity (Dee et al., 2015; Thompson et al., 2011). We use surface temperature and salinity output from the Community Earth System Model Last Millennium Ensemble (CESM-LME) (Otto-Bliesner et al., 2016) to model pseudocoral $\delta^{18}\text{O}$ and SST derived from Sr/Ca ($\text{SST}_{\text{Sr/Ca}}$). The model is applied to two sites in the central (Kiritimati) and southwest Pacific (Vanuatu) as case studies to demonstrate the sub-components of our PSM, and then our pseudoproxy network is expanded to span the broader tropical Pacific.

Our specific objective is to identify how uncertainties associated with (1) analytical and calibration errors, (2) variable growth rates, and (3) age modeling assumptions impact interannual variance and the ability of a pseudocoral to capture decadal and longer (decadal+) changes in ENSO variability. Although precise month-to-month SST variations in the Niño 3.4 region are a common target for ENSO studies, this is challenging for paleoclimate studies because of temporal uncertainties in proxy records (Emile-Geay et al., 2013a, 2013b). Thus, we focus on how various coral processes impact estimates of decadal+ changes in ENSO variability in coral paleoclimate reconstructions. Section 2 describes the coral PSM framework and the various submodels. Section 3 provides results and discusses the impact of the three coral uncertainties on interannual variance, as well as a coral's ability to capture changes in ENSO variability. The conclusions are provided in section 4.

2. A New Coral PSM

Proxy system models are tools used to evaluate the contribution of local environmental signals and their variability on the measured proxy record

and have been widely employed to assess uncertainties in paleoclimate data for a variety of geological archives and proxy types (e.g., Comboul et al., 2014; Dee et al., 2015, 2018; Evans et al., 2007, 2013; Herron & Langway, 2017; Johnsen et al., 2000; Partin et al., 2013; Roden et al., 2000; Thompson et al., 2011; Wong & Breecker, 2015). This study introduces a coral PSM that builds upon previous work and adds new layers of complexity by incorporating uncertainties related to the following:

1. variable growth rates experienced when sampling a coral along the maximum growth axis;
2. analytical and calibration errors; and
3. seasonal chronological uncertainties associated with transforming coral geochemical data from the depth to the time domain (herein referred to as the age model).

The additions presented here adhere to the PSM submodel framework described in Evans et al. (2013) where a PSM consists of environment, sensor, archive, and observation subcomponents (Figure 1). This is the first study to include an archive-based coral PSM with a variable growth rate algorithm. Analytical and calibration errors as well as the age model assumptions fall within the observation subcomponent of the PSM.

Our coral PSM allows the user to run different permutations of the various archive and observation submodels (Figure 1 arrows). For example, to isolate the impact of age modeling assumptions the user can solely perturb pseudocoral $\delta^{18}\text{O}$ or SST derived from Sr/Ca ($\text{SST}_{\text{Sr/Ca}}$) with the age model algorithm (Figure 1). The full coral PSM herein refers to first perturbing the coral sensor output with the variable growth rate

algorithm, followed by analytical and/or calibration errors, and the then age modeling algorithm (follow the center arrows in Figure 1). With this framework we can also use Monte Carlo methods to generate many realizations of pseudocoral $\delta^{18}\text{O}$ or $\text{SST}_{\text{Sr/Ca}}$ in order to quantify the uncertainty in coral-inferred estimates of variance. This study focuses on how various uncertainties impact interannual variance, a leading time scale of interest for coral-based paleoclimatology.

2.1. Coral PSM Input Variables

In this study, we use surface temperature and salinity output from the CESM-LME 850 control (Otto-Bliesner et al., 2016) as the environmental inputs to demonstrate how the new coral PSM quantifies how the coral archive affects interannual variance in coral climate reconstructions. The environmental inputs for the coral PSM are SST, sea surface salinity (SSS), and $\delta^{18}\text{O}_{\text{sw}}$ if available (Figure 1). These climate variables can be from instrumental observations or model output, though we choose to only use model output for this study. In this study, we use surface temperature and salinity output from the CESM-LME 850 control (Otto-Bliesner et al., 2016) as the environmental inputs. The CESM-LME uses version 1.1 of CESM with the Community Atmospheric Model Version 5, CESM1(CAM5) (Hurrell et al., 2013). The CESM-LME has $\sim 2^\circ$ resolution for the atmosphere and $\sim 1^\circ$ resolution for the ocean. We use the 2-m surface temperature output from the atmospheric model (CAM5), which will equal SST over the ocean. The surface salinity (0–10 m depth) output was gridded to the same $\sim 2^\circ$ resolution as the atmospheric components to facilitate forward modeling coral $\delta^{18}\text{O}$ as a linear combination of SST and SSS (section 2.3.1).

We focus on CESM as this model exhibits realistic ENSO dynamics (DiNezio et al., 2017; Wu et al., 2019), and there are no changes in external forcing throughout the CESM-LME 850 control simulation (Otto-Bliesner et al., 2016), hence all of the changes in interannual variability within the simulation are unforced. The 850 control is also sufficiently long (1,156 years) to sample across a wide range of internal variability, which is not possible in the short instrumental record (Stevenson et al., 2010; Wittenberg, 2009). Implementing our new coral PSM using CESM-LME allows us to quantify how different assumptions and uncertainties inherent to the coral archive impact interannual variance in a geochemical time series, while minimizing the impacts of a stationarity assumption by removing any effects that could result from external forcing. Here, the proxy uncertainties are evaluated within the simulated climate generated by the model, such that we constrain ourselves to the CESM-LME's simulation of tropical Pacific variability, including ENSO. Due to model biases, the spatial patterns observed using the CESM-LME may not be strictly comparable to other models or instrumental observations, but the general results about how the three coral uncertainties impact interannual variability within the framework of CESM are broadly applicable to other environmental inputs. Due to model biases, we caution future users of the PSM to avoid direct point-to-point comparisons between coral observations and climate model output from a single grid point. Care must be taken to select a region in the model that best matches the climate conditions observed at the proxy site.

2.2. Case Studies: Kiritimati and Vanuatu

ENSO involves basin-scale atmospheric and oceanic interactions across the tropical Pacific, with the largest interannual signal occurring in the central and eastern equatorial Pacific. In contrast, coral heads are point source locations (on the scale of meters) that are impacted by both regional and local climate processes. Thus, there needs to be a demonstrated link between climate variability at the individual reef site and ENSO. Modern and paleo-ENSO studies have targeted sites within the Niño 3.4 region (Cobb et al., 2013; Emile-Geay et al., 2016), as well as sites in the eastern, western, and southwest Pacific that are sensitive to changes in ENSO variability (Hereid, Quinn, & Okumura, 2013). For example, the western and southwest Pacific contain a large number of islands that are home to abundant modern and fossil coral heads for paleoclimate studies (Cole et al., 1993; DeLong et al., 2012; Gorman et al., 2012; Hereid, Quinn, Taylor, et al., 2013; Jimenez et al., 2018; Kilbourne et al., 2004; Linsley et al., 2006; and many others).

We choose two end-member localities at Kiritimati (2°N , 157°W) and Vanuatu (16°S , 167°E) to apply our coral PSM for testing how different processes and uncertainties inherent to coral-based paleoclimatology impact interannual variance. Kiritimati, located in the central equatorial Pacific, has a small annual cycle and a large interannual response to ENSO, whereas Vanuatu, located within the South Pacific Convergence Zone, has a larger annual cycle and a smaller interannual response to ENSO. In all instances,

when selecting the environmental input for the coral PSM, we use the model output from the grid point closest to the selected sites.

2.3. Coral Sensor Models

2.3.1. Pseudocoral $\delta^{18}\text{O}$

We use the coral sensor model of Thompson et al. (2011) to forward model mean-removed pseudocoral $\delta^{18}\text{O}$ anomalies ($\Delta\delta^{18}\text{O}_{\text{pseudocoral}}$) as a linear combination of SST and $\delta^{18}\text{O}_{\text{sw}}$ or salinity anomalies:

$$\Delta\delta^{18}\text{O}_{\text{pseudocoral}} = a_1\Delta\text{SST} + \Delta\delta^{18}\text{O}_{\text{sw}} \quad (1)$$

$$\Delta\delta^{18}\text{O}_{\text{pseudocoral}} = a_1\Delta\text{SST} + a_2\Delta\text{SSS} \quad (2)$$

The Δ symbol indicates the removal of the mean of the full-length SST and SSS/ $\delta^{18}\text{O}_{\text{sw}}$ input time series such that the resulting $\delta^{18}\text{O}_{\text{pseudocoral}}$ anomalies are centered around zero. The coefficient a_1 is based on the inverse SST dependence that arises from thermodynamic fractionation (Epstein et al., 1953). The temperature dependence for $\delta^{18}\text{O}$ at individual coral sites may range from -0.10 to $-0.34\text{‰}/^\circ\text{C}$ (Evans et al., 2000), whereas studies that synthesize the results from multiple locations report values of -0.20 (Evans et al., 2000) and -0.22 (Lough, 2004), which are close to the inorganic slope of $-0.22\text{‰}/^\circ\text{C}$ (Epstein et al., 1953). Here we use a slope $-0.22\text{‰}/^\circ\text{C}$ for a_1 as used in Thompson et al. (2011).

SSS and $\delta^{18}\text{O}_{\text{sw}}$ are often assumed to be linearly proportional as they are impacted by similar precipitation, evaporation, and advection processes (LeGrande & Schmidt, 2006). We use Equation 2 and approximate a_2 using observed $\delta^{18}\text{O}_{\text{sw}}$ -SSS slopes determined from basin-scale regression analysis (LeGrande & Schmidt, 2006). Limited $\delta^{18}\text{O}_{\text{sw}}$ and SSS observations (LeGrande & Schmidt, 2006), spatiotemporal variability in the $\delta^{18}\text{O}_{\text{sw}}$ -SSS relationship (Conroy et al., 2017), or subgrid processes affecting $\delta^{18}\text{O}_{\text{sw}}$ (Stevenson et al., 2015) can lead to large errors on interannual variance (Russon et al., 2015; Stevenson et al., 2013) and hinder direct comparison between forward modeled pseudocorals and coral proxy observations. That said, since our study focuses on the impact of other processes on interannual variance we define a_2 as 0.27 for tropical Pacific latitudes north of 5°S (e.g., Kiribati), and 0.45 for latitudes south of 5°S (e.g., Vanuatu) as defined in LeGrande and Schmidt (2006).

2.3.2. Pseudocoral SST Derived From Sr/Ca ($\text{SST}_{\text{Sr/Ca}}$)

The inverse relationship between coral Sr/Ca and temperature is an established proxy for reconstructing SST (Beck et al., 1992; Corrège, 2006; Gagan et al., 2000; Lough, 2010; Quinn & Sampson, 2002). Slope values for the linear Sr/Ca-SST transformation typically fall within the -0.06 ± 0.01 ($\pm 1\sigma$) mmol/mol/ $^\circ\text{C}$ range for the Indo-Pacific (Corrège, 2006). Uncertainties in the Sr/Ca-SST calibration can yield errors in the SST reconstruction up to 0.35°C ($\pm 2\sigma$) (Quinn & Sampson, 2002), although this uncertainty may be larger based on interlaboratory comparisons (Hathorne et al., 2013) and reproducibility studies (Sayani et al., 2019). A published coral Sr/Ca sensor model does not exist at the time of this study but it could be incorporated into our coral PSM framework in the future. Given that a variety of slope values are published in the literature, in this study we assume that the original SST input to the coral PSM is a reasonable approximation of SST derived from coral Sr/Ca ($\text{SST}_{\text{Sr/Ca}}$). This assumption helps circumnavigate some of the challenges associated with developing a universally applicable coral Sr/Ca sensor model. Importantly, this assumption also helps facilitate comparison between $\text{SST}_{\text{Sr/Ca}}$ processed using the coral PSM algorithms and the original, unperturbed SST output from the model. The error in the Sr/Ca-SST calibration is considered in our PSM, as further discussed in section 2.5.1.

2.4. Coral Archive Model: Variation in Coral Growth Rates

Subseasonal resolution is a goal of many coral paleoclimate studies that seek to quantify changes in interannual variance. However, a coral's growth rate may vary both within and between years. For example, a *Porites* coral growing an average of 1.2 cm/year would achieve approximately monthly resolution if sampled in 1 mm increments. Although monthly resolution is targeted, one sample of coral powder may average 2–3 weeks (-2σ) of time when the coral is growing faster, or 5–6 weeks ($+2\sigma$) when the coral is growing slower. Due to variable growth rates, the net effect of equal sampling in the depth domain will lead to unequal sampling in the time domain. We use our coral PSM to assess how variations in coral growth impact

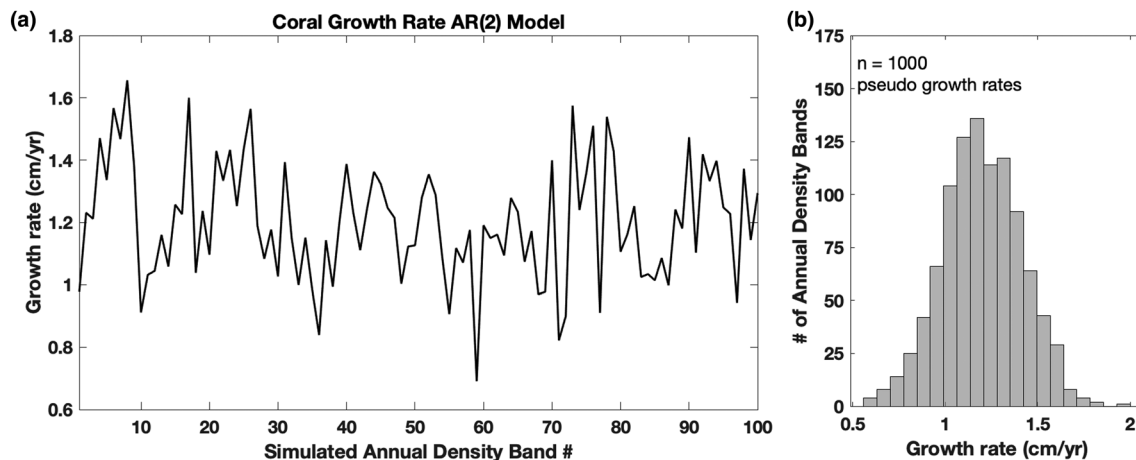


Figure 2. Simulated annual coral growth rates (cm/year). (a) A randomly generated realization of simulated growth rates for 100 pseudocoral annual density bands. The growth rates are simulated using an autoregressive order 2, AR(2), model with lag coefficients and variance parameters determined from measured *Porites* corals from the Southwest Pacific (section 2.4). This figure shows one randomly generated realization of the AR(2) simulated growth rates. We note that the variable growth rate model could be run multiple times to generate n realizations that are subsequently used to stretch and compress the original input to the coral PSM. (b) Histogram of modeled pseudo *Porites* annual growth rates (1.2 ± 0.2 cm/year, $\pm 1\sigma$). The pseudocoral annual growth rates are used to stretch and compress the environmental inputs to mimic how equal sampling in the depth domain can yield to unequal sampling in the time domain.

the variance of a resulting geochemical time series when the coral is sampled at a fixed sampling resolution (e.g., 1 mm).

High-precision calipers were used to measure the annual growth rates of nine modern and fossil *Porites* cores from Vanuatu to generate a distribution of growth rates with a mean of 1.2 ± 0.2 cm/year ($\pm 1\sigma$). The measured growth rate values are consistent with the reported average values for *Porites* corals from other regions of the tropical Pacific (Cobb et al., 2013). We incorporate variable growth rates into the coral PSM using an autoregressive order 2, AR(2), model since the measured annual growth rates are serially correlated and cannot be modeled with an independent error term. The lag 1 and 2 correlation coefficients (0.25 and 0.20, respectively), and the standard deviation (0.2 cm/year) for the AR(2) model are based on the nine measured *Porites* corals. The AR(2) model is used to generate a series of annual growth rates (Figure 2a). The distribution of simulated growth rates (Figure 2b) is consistent with the measured coral growth rates given a large n , as the simulated growth rates are pulled from a distribution based on measured growth rates. The parameters for the AR(2) model can easily be adjusted for different species or for a different median and/or standard deviation of growth rates.

A single realization of the AR(2) model provides a transformation from the time to the depth domain. One random realization for SST and forward modeled $\Delta\delta^{18}\text{O}_{\text{pseudocoral}}$ is provided at Kiritimati and Vanuatu as an illustrative example of how the algorithm works (Figures 3a–3d). The pseudocoral annual growth rates are used to stretch and compress the original PSM inputs to mimic how equal sampling in the depth domain can yield to unequal sampling in the time domain. The net effect of the variable growth rate algorithm is that the pseudocoral output looks stretched and compressed relative to the original input. Monte Carlo methods are used to generate n number of random realizations of the AR(2) model that are then used to stretch and compress the original, unperturbed SST or $\Delta\delta^{18}\text{O}_{\text{pseudocoral}}$ input time series n number of times.

2.5. Coral Observation Models

2.5.1. Analytical and Calibration Errors

Monte Carlo methods are also used to randomly generate 1,000 $\Delta\delta^{18}\text{O}_{\text{pseudocoral}}$ time series perturbed with analytical errors, and 1,000 SST_{Sr/Ca} time series perturbed with the combined impact of analytical and calibration errors. The analytical and calibration errors are both modeled as Gaussian white noise, such that they sum accordingly (Figures 3e–3h). For $\Delta\delta^{18}\text{O}_{\text{pseudocoral}}$, analytical errors are taken as 0.20‰ ($\pm 2\sigma$), a value typical of laboratory analytical precision. For coral SST_{Sr/Ca}, we incorporate the combined effect of the analytical instrument error, as well as the linear calibration error associated with transforming coral

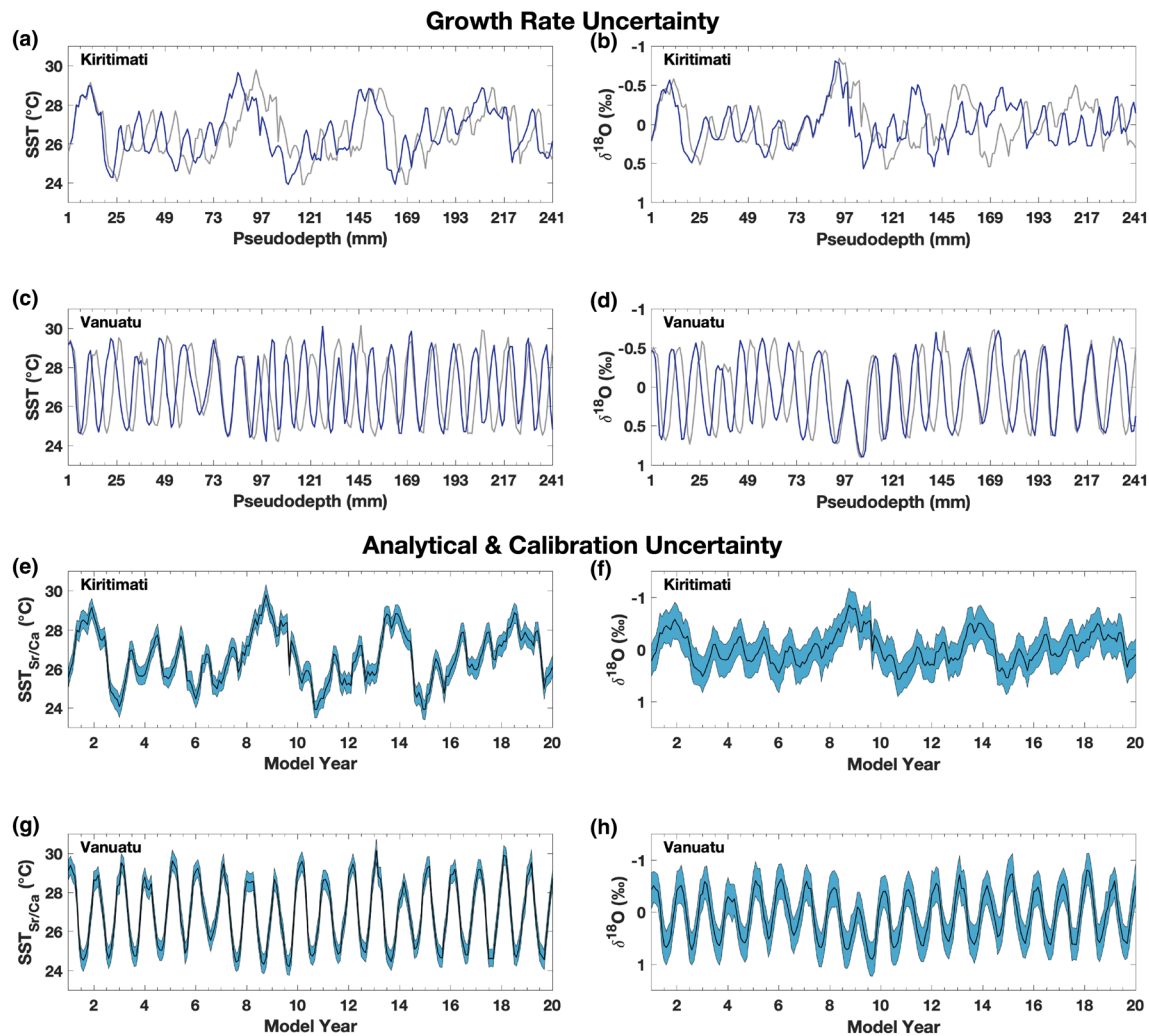


Figure 3. Impact of variable growth rates and analytical and calibration errors on environmental signals. (a–d) Blue curves depicts the original SST (a, c) and $\Delta\delta^{18}\text{O}_{\text{pseudocoral}}$ (b, d) inputs transformed from the time to the depth domain using a realization of the AR(2) variable growth rate model. Gray curves indicate the original inputs transformed to the depth domain using a constant transformation of 1.2 cm/year (i.e., no variable growth rates) for the model grid points closest to Kiritimati (a, b) and Vanuatu (c, d). Model output in this and all subsequent figures are from the CESM-LME 850 control (Otto-Bliesner et al., 2016) (section 2.1). $\Delta\delta^{18}\text{O}_{\text{pseudocoral}}$ (‰, VSMOW) in this and all subsequent figures is generated using the sensor model of Thompson et al. (2011) (section 2.3.1). We refer the reader to Friedman and O’Neil (1977) for the conversion to ‰, VPDB. (e, g) Pseudocoral $\text{SST}_{\text{Sr/Ca}}$ perturbed with the combined effect of analytical and calibration errors ($\pm 0.30^\circ\text{C}$, 2σ ; section 2.5.1) at the model grid points closest to Kiritimati (e) and Vanuatu (g). (f, h) $\Delta\delta^{18}\text{O}_{\text{pseudocoral}}$ perturbed with analytical error ($\pm 0.20\text{‰}$, 2σ ; section 2.5.1) for Kiritimati (f) and Vanuatu (h). Black line in (e)–(h) indicates the unperturbed environmental inputs for the selected sites, and the blue shading represents the spread of forward modeled pseudocoral time series ($n = 1,000$). For illustrative purposes, each panel includes a 20-year subset of the 850 control to show how variable growth rates and analytical/calibration errors impact the original inputs.

Sr/Ca into SST. Previous studies identified that the net effect of analytical and calibration errors can cause uncertainties of $\sim 0.30^\circ\text{C}$ in Sr/Ca–SST reconstructions ($\pm 2\sigma$) (Alibert & McCulloch, 1997; Quinn & Sampson, 2002; Schrag, 1999). The original SST environmental inputs are thus perturbed with Gaussian white noise that includes the combined impact of analytical and calibration errors (0.30°C , $\pm 2\sigma$). The error term for $\text{SST}_{\text{Sr/Ca}}$ can be changed within the PSM framework to account for larger analytical and calibration error terms (Corrège, 2006; DeLong et al., 2013; Hathorne et al., 2013; Sayani et al., 2019) based on user need.

2.5.2. Monthly Coral Chronology

The creation of an age model in coral paleoclimate studies requires the measured climate indicator (proxy) be transformed from the depth into the time domain. We investigate the impact of key age modeling assumptions on interannual variance. We note that the assumptions discussed here are different than the

uncertainties that arise from missing or double counting years in annually banded archives (Comboul et al., 2014) that have been previously incorporated into existing PSM frameworks (Dee et al., 2015).

The chronology for coral data that has been sampled at approximately monthly resolution typically uses annual cyclicity in the data to constrain a relative chronology. For coral Sr/Ca, larger values indicate cooler temperatures, while smaller values indicate warmer temperatures (Beck et al., 1992; Smith et al., 1979; Weber, 1973). For coral $\delta^{18}\text{O}$, surface conditions often constructively interfere such that more negative extrema indicate warmer and/or fresher conditions, while more positive extrema indicate cooler and/or more saline conditions (Corrège, 2006; Fairbanks et al., 1997; Lough, 2010), though exceptions may occur. When constructing an age model, the peaks and troughs in the coral geochemical data are assigned a specific calendar month based on knowledge about the climatology at the site. For example, if the site on average experiences the warmest SST during June and the coolest SST during December, then the Sr/Ca minima are assigned the month of June and the Sr/Ca maxima are assigned the month of December. Coral $\delta^{18}\text{O}$ is a function of SST and the $\delta^{18}\text{O}_{\text{sw}}$ (SSS), so the input for the climatological extrema in $\delta^{18}\text{O}$ may be dominated by temperature, salinity, or a combination of the two variables. Once identifying all the geochemical extrema, the coral data are interpolated to achieve evenly spaced monthly resolution. The resulting relative age model can be further refined by overlapping the coral record with instrumental observations (modern corals only) and with high-precision ^{230}Th ages that serve as absolute chronological constraints with errors $\sim 1\%$ of the age (Cheng et al., 2013; Shen et al., 2012).

We developed a MATLAB® algorithm to standardize coral age modeling and have made it publicly available. The age model algorithm assumes that the coral was optimally sampled along the maximum growth axis (DeLong et al., 2013) at subseasonal resolution. The coral geochemical data (in the depth or sample-number domain) is the first required input for the age model algorithm. There are several additional inputs supplied by the user based on their individual lab procedures. First, the user must provide the estimated sampling resolution of the coral (e.g., 10–14 samples per annual growth band). The user must also supply the calendar month that corresponds to the annual peaks and trough in the geochemical data. For Sr/Ca (or $\text{SST}_{\text{Sr/Ca}}$ as in this study), this input would be the climatological warmest and coolest months at the coral site. The climatological month assignment can be determined from instrumental observations or model output for past time intervals when the annual cycle is not known. The target temporal resolution for the age modeled output defaults to monthly resolution (12 points/year), but this parameter can be changed by the user if desired.

We demonstrate the utility of the age model algorithm using SST from the grid points nearest to Vanuatu and Kiritimati as illustrative examples (Figures 4 and 5). The age modeling approach for $\Delta\delta^{18}\text{O}_{\text{pseudocoral}}$ is identical and produces similar results (Figures S1 and S2 in the supporting information). The age model uses a standard peak finding algorithm in the MATLAB® software (findpeaks) to identify local minima and maxima (i.e., inflection points) in the geochemical data (Figures 4c and 5c), herein referred to as critical points. To identify the critical points the input coral data are first 2-month low-pass filtered to smooth out high-frequency noise and better-illuminate the annual cyclicity in the data. The peak-finding algorithm then finds all of the peaks and troughs in the low-pass filtered data, and then ranks the critical points by their prominence (i.e., height) as well as their location relative to other prominent extrema. This ranking scheme ensures that the critical points are not spaced too closely or too far apart given the original sampling resolution of the data. The locations of the highest ranked peaks/troughs in the low-pass filtered time series are then mapped to the original input data set. The selected critical points are then assigned a calendar month based on the climatological input (Figures 4a and 5a). The data are then interpolated to monthly resolution using the geochemical extrema as tie points (Figures 4f and 5f). Our interpolation scheme uses a piecewise linear transformation (Fritsch et al., 1980).

The algorithm also contains an option to constrain the number of years based on an approximate number of annual density bands visible in a coral's X-ray image. The number of years constraint is often not necessary for sites with a clear annual cycle (e.g., the southwest Pacific), but may be necessary for sites with a small and/or noisy annual cycle (e.g., the equatorial Pacific). The age model algorithm is deterministic, meaning that for a given Sr/Ca or $\delta^{18}\text{O}$ input series the age model will find a single solution that meets the constraints provided by the user. In the context of the full coral PSM presented here, multiple realizations of age modeled pseudocoral output can be generated by first perturbing the PSM input with the variable growth

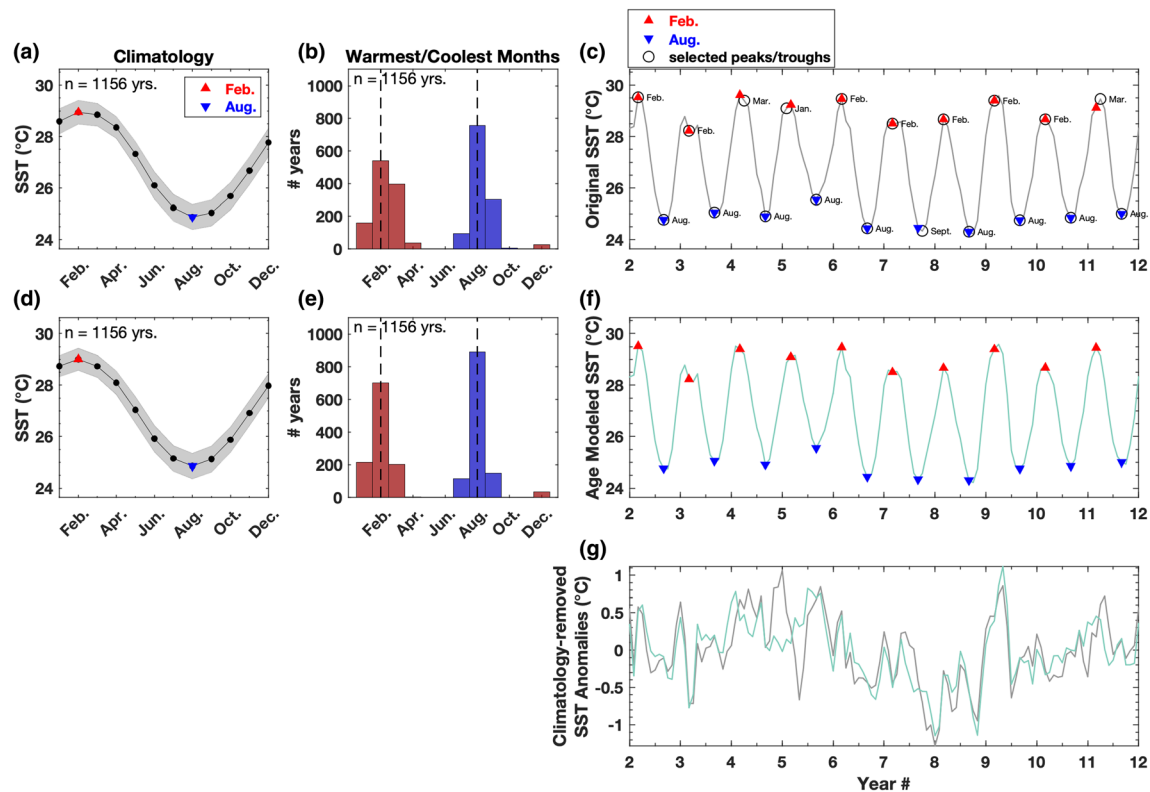


Figure 4. Age modeling of pseudocoral SST at Vanuatu. Climatology (black) $\pm 1\sigma$ (shading) for the original (a) and age-modeled (d) SST output for the grid point nearest Vanuatu in the CESM-LME 850 control ($n = 1,156$ years). Histogram of the warmest (red bars) and coolest (blue bars) month for each individual year in the (b) 850 control and the (e) age modeled SST output. The climatological warmest/coolest months are indicated with dashed vertical lines in (b, e). (c) 10 years of the (c) unperturbed monthly SST and the (f) age modeled monthly SST at Vanuatu. Triangles in (a), (c), (d), and (f) indicate the climatological warmest (February) and coolest (August) months. The black circles in (c) indicate the peak/troughs identified by the age model algorithm, and the adjacent text labels indicate the calendar month at each critical point. (g) Monthly SSTA for the original input (black) and age modeled pseudocoral SST (teal). In this and all subsequent figures, anomalies are with respect to the climatology of the full-length control run. The warmest/coolest month distributions in (b) and (e) are wider than a single month and is directly related to a loss of interannual variance in (g).

rate algorithm (section 2.4). Alternatively, the user can follow the protocol of the Comboul et al. (2014) banded age model and perturb the number of years constraint within error.

3. Results and Discussion

After developing the submodels of our coral PSM, including the three additions that model variable growth rates in the context of sampling, analytical and calibration errors, and age model assumptions, we now apply the model to constrain the climatic impacts. These three sources of uncertainty alter the input climate signals and impact estimates of interannual variance and ENSO variability inferred from the pseudocorals. Tropical reefs are point sources for paleoclimate reconstructions; by contrast, with climate model output the coral PSM can be run at every grid point in the tropical Pacific to identify regional patterns. Broad regions of the tropical Pacific exhibit distinct patterns when the original environmental inputs are perturbed using the coral PSM. We separate the identified patterns into three subsections: changes in the standard deviation of monthly anomalies as recorded by corals, decadal and longer changes in ENSO variability, and decadal and longer changes in ENSO variability as recorded by corals.

3.1. Quantifying Changes in Interannual Variability: Monthly Standard Deviation

The percent change in standard deviation between the perturbed pseudocorals and the original (unperturbed) SST or $\Delta\delta^{18}\text{O}_{\text{pseudocoral}}$ climatology-removed anomalies is a method used to quantify changes in interannual variance. The percent difference between the unperturbed anomalies and the anomalies that result from that PSM (Figure 6) is calculated using the median standard deviation value for n realizations of

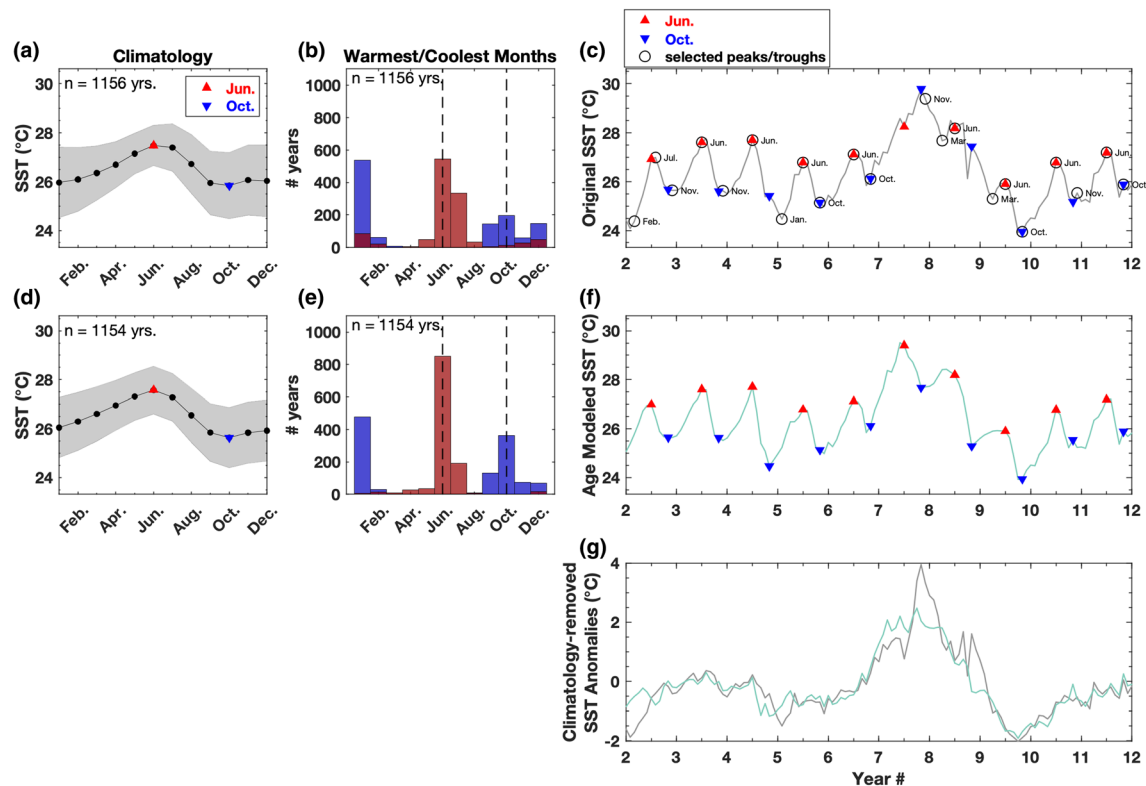


Figure 5. Age modeling of pseudocoral SST at Kiritimati. Same as Figure 4 except for the grid point nearest to Kiritimati. Triangles in (a), (c), (d), and (f) indicate the climatological warmest (June) and coolest (October) months. Years with strong El Niño events (e.g., model years 8 and 9) have a reduced annual cycle and a small and/or absent trough during boreal winter, leading to incorrect month assignment in (f) that results in a reduction in interannual variance in anomaly space (g).

the perturbed pseudocoral monthly anomaly time series. The percent change in standard deviation highlights site dependencies in the results. The changes in interannual variance between the original environmental inputs and the coral PSM output at a given location is linked to both the amplitude of the interannual signal and the annual cycle. Analytical and calibrations errors (section 2.5.1) cause a systematic increase in interannual variance for pseudocoral SST_{Sr/Ca} (Figure 6b) and $\Delta\delta^{18}\text{O}_{\text{pseudocoral}}$ (Figure 6f) compared to the original environmental inputs. Regions of the Pacific with a large interannual signal (Figures 6a and 6e) are less impacted by analytical/calibration errors compared to regions with a smaller interannual signal.

For the age modeling assumptions, we first assess how the algorithm (section 2.5.2) impacts interannual variance locally at Kiritimati and Vanuatu before extending the analysis to the broader tropical Pacific. SST from the grid points nearest to Vanuatu and Kiritimati are provided as illustrative examples (Figures 4 and 5; section 2.5.2). The results for $\Delta\delta^{18}\text{O}_{\text{pseudocoral}}$ are similar (Figures S1 and S2). Simulated SST at Vanuatu shows a clear annual cycle with the climatological warmest month occurring in February and the climatological coolest month in August (Figure 4a). The algorithm does well in identifying the timing of the austral warm/cool season peaks at Vanuatu (Figure 4c, black circles). The algorithm assigns the critical points the climatological warmest (February) and coolest (August) months, and the data are linearly interpolated between the critical points to generate the age modeled time series (Figure 4f). At Kiritimati, where the annual cycle is smaller (Figure 5a), the algorithm encounters more difficulties in identifying seasonal extrema due to the relatively large amplitude of interannual variability, as compared to the amplitude of the seasonal cycle (Figures 5b and 5c). Uncertainty in the age model of a coral record results when the common assumption that the months of the climatological extrema do not change is violated.

To show how this uncertainty manifests, we show the spread in the distribution of the warmest and coolest months. Although February and August are climatologically the warmest and coolest months at Vanuatu,

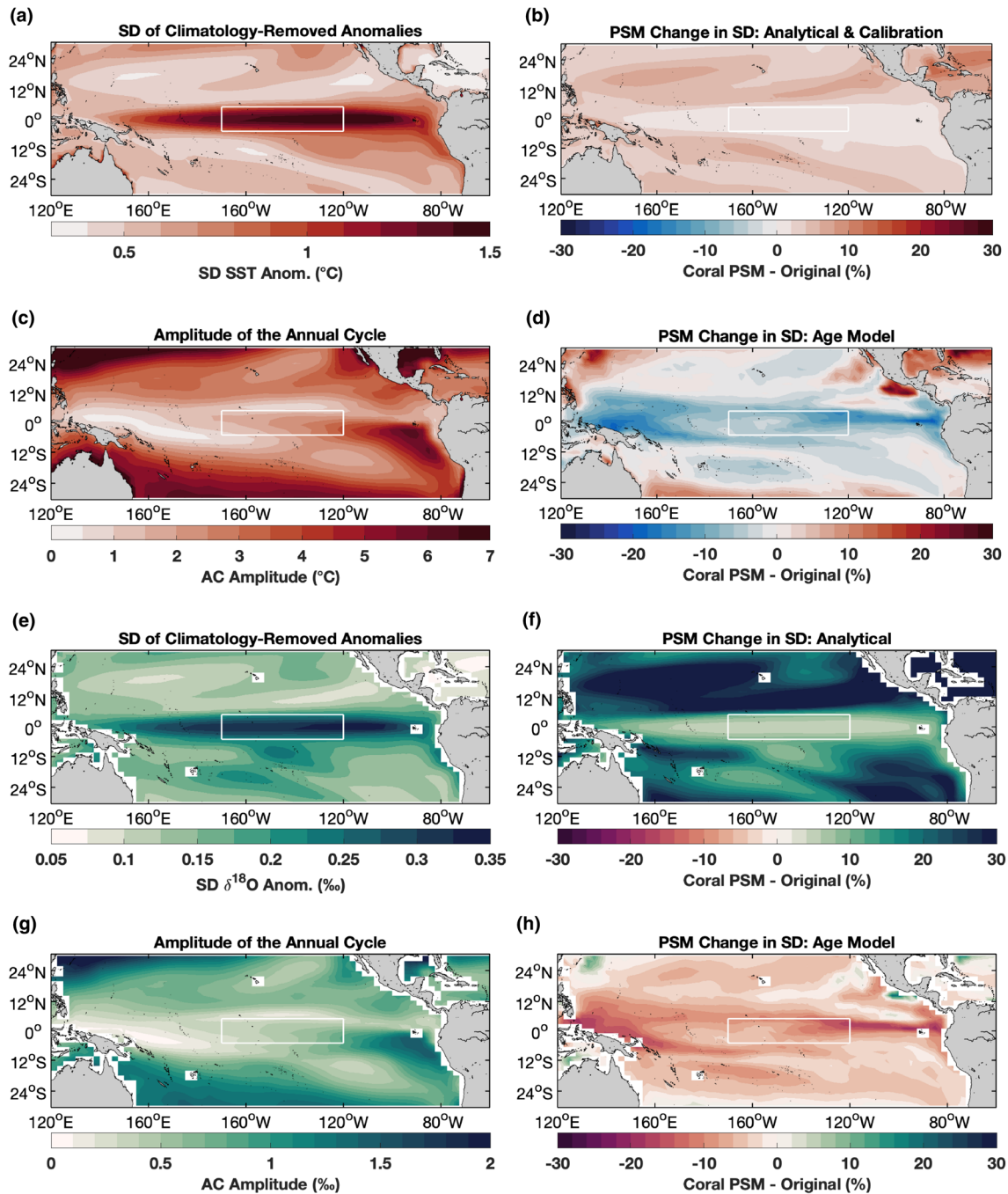


Figure 6. Pseudocoral SST_{Sr/Ca} and $\delta^{18}\text{O}$ changes in interannual variance. (a) Standard deviation (SD) of monthly SSTa in the LME 850 control. Warm colors highlight regions with the largest interannual signal. (b) Percent difference in SD between pseudocoral SST_{Sr/Ca} anomalies perturbed with analytical and calibration errors and the SD of the unperturbed SST anomalies. (c) Amplitude of the annual SST cycle in the LME 850 control. (d) Percent change in SD between age modeled pseudocoral SST_{Sr/Ca} anomalies and the original, unperturbed SST anomalies. (e) SD of monthly forward modeled $\Delta\delta^{18}\text{O}_{\text{pseudocoral}}$. (f) Percent difference in SD between pseudocoral $\delta^{18}\text{O}$ anomalies perturbed with analytical errors and the SD of the unperturbed $\Delta\delta^{18}\text{O}_{\text{pseudocoral}}$ anomalies. (g) Amplitude of the annual $\Delta\delta^{18}\text{O}_{\text{pseudocoral}}$ cycle in the 850 control. (h) Percent change in SD between age-modeled pseudocoral $\Delta\delta^{18}\text{O}$ anomalies and the original, unperturbed $\Delta\delta^{18}\text{O}$ anomalies. The percent difference in SD for the full-length time series (~1,156 years) is reported. The SD for the coral PSM output is the median of 1,000 realization in (b) and (f) and 1 realization of the deterministic age model (d, h). The Niño 3.4 region is outlined by a white box (a–h). The changes in interannual variance from analytical/calibration errors (b, f) is inversely related to the magnitude of the interannual signal (a, e), whereas the change in variance from age modeling (d, h) is linked to the amplitude of the annual cycle (c, g). Colormaps in this and all subsequent maps use the cmocan: colormaps for oceanography toolbox (Thyng et al., 2016).

there are years in which other months are the warmest or coolest (Figure 4b). That said, the overall spread in the distribution of the warmest and coolest months at Vanuatu (Figure 4b) is narrow. Since the distribution is narrow the age model algorithm has more success in identifying the correct calendar month in the extrema in the time series. That said, there is still an incorrect month assignment in the age model. For example, March is the actual warmest month in model year 4, but the age model algorithm assigns the month of February to the SST peak (Figure 4c). In contrast, the distribution of the simulated warmest/coolest months at Kiritimati (Figure 5b) is broad, such that there is a large error in assigning the correct calendar month to the extrema. In worst-case scenarios, model years with strong El Niño events have a small, nearly absent annual cycle with SSTs during boreal winter (December–February) surpassing the climatological summertime maximum values typically experienced in June. Without constraining the approximate number of years, it is easy to miss weak troughs during boreal winters with El Niño events, and therefore miss years. These age model assumptions can yield large differences (~10–30%) in interannual variance when the climatology of the age modeled time series (Figures 5d and 5f) is removed from incorrectly assigned months to generate SST anomalies (Figure 5g).

Globally, the increase in annual cycle regularity induced by the age model (section 2.5.2) broadly tends to cause a decrease in interannual variance across most of the tropical Pacific (Figures 6d and 6h). The largest percent change in standard deviation occurs in the central Pacific and eastern Pacific cold tongue regions where ENSO events can lead to climatologically coolest months that are warmer than the climatologically warmest months. It is thus difficult to identify a trough in the geochemical data and accurately assign a month to the data when age modeling (section 2.5.2). The age model effects are particularly exacerbated in the CESM-LME due to biases in the amplitude of ENSO events (Otto-Bliesner et al., 2016). Conversely, pseudocorals generated at sites with a larger annual cycle and less variable distribution of warmest and coolest months have a smaller reduction in interannual variance compared to the original environmental input (Figures 6d and 6h). Outside of the tropics, however, sites that have multiple consecutive months with approximately the same average SST value experience an increase in variance (Figure 6d). For a given site, the magnitude of the percent change is typically larger for $\Delta\delta^{18}\text{O}_{\text{pseudocoral}}$ compared to SST given that $\delta^{18}\text{O}$ is multivariate and may have contributions from SSS that may be a few months out of phase with SST (e.g., Gorman et al., 2012) (Figure 6d versus Figure 6h).

The percent change in standard deviation for the full coral PSM (Figure 7) reveals the tradeoff between interannual variability and the amplitude of the annual cycle. At locations with the strongest interannual signal (equatorial sites), the loss of variance due to the age model assumptions, that is, incorrect months assigned to extrema, exerts the dominant influence on interannual variance for pseudocoral $\text{SST}_{\text{Sr/Ca}}$ (Figure 7a) and $\delta^{18}\text{O}$ (Figure 7b). Although age model uncertainty also causes a decrease in variance in regions like the southwest Pacific, the relative magnitude of the change is compensated by the increase in variance that results from analytical and calibration errors. Our results highlight that the different processes and assumptions inherent to coral-based studies exert sizable impacts on pseudocoral interannual variance and that the relative contributions are site dependent. While changes in the monthly standard deviation of an individual anomaly time series can show longer-term changes in ENSO (Wittenberg, 2009), uncertainties in coral climate reconstructions (Emile-Geay et al., 2013a, 2013b) preclude such a reconstruction back in time, thus warranting an alternative metric for paleo-ENSO studies.

3.2. Quantifying Changes in ENSO Variability: Decadal+

This section evaluates the impact of coral uncertainties on reconstructing changes in ENSO variability through time. Although precise month-to-month variations of SST in the Niño 3.4 region are a sought-after target for ENSO studies, this is difficult to reconstruct back in time using a limited number of coral proxy records with age uncertainties. Previous studies have used sophisticated statistical techniques on corals from the last millennium and still had an appreciable degree of uncertainty in the reconstruction (Emile-Geay et al., 2013a, 2013b). Fossil corals with absolute age errors on the order of 1% make a month-to-month reconstruction virtually impossible on 10^3 years and longer time scales. We address this challenge by building upon the procedure suggested in Trenberth (1997) and use descriptive statistics and probability theory to quantify changes in ENSO variability on the time scale of decades. Indeed, the technique of looking at changes in ENSO over windows in the past has already been employed using corals from the central Pacific (Cobb et al., 2013).

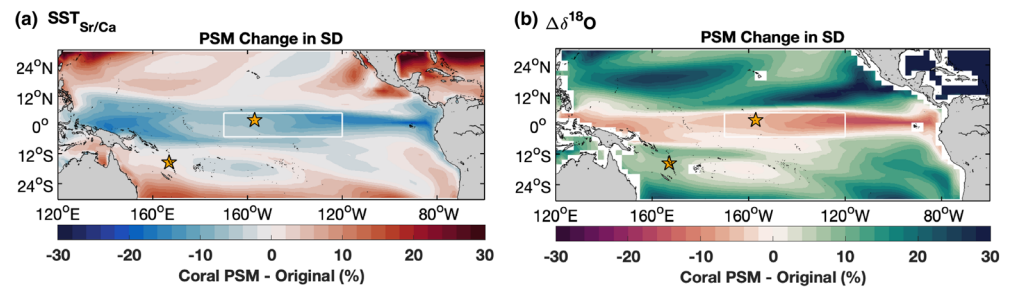


Figure 7. Changes in interannual variance for the full coral PSM. Percent difference in SD between pseudocoral (a) $SST_{Sr/Ca}$ and (b) $\Delta\delta^{18}O$ anomalies perturbed with variable growth rates, analytical/calibration errors, and the age modeling algorithm, and the original, unperturbed environmental input ($n = 100$ realizations). Selected sites at Kiritimati ($2^{\circ}N$, $157^{\circ}W$) in the Central Pacific, and Vanuatu ($16^{\circ}S$, $167^{\circ}E$) in the Southwest Pacific are indicated with gold stars. The white box outlines the Niño 3.4 region. The percent change in SD for the full coral PSM reveals the tradeoff between interannual variability and the amplitude of the annual cycle (Figure 6).

We formalize this technique to quantify changes in ENSO variability using climatology-removed SST anomalies averaged across the Niño 3.4 region (Figure 6, box). The time series is restricted (Figure 8a) to the first 200 years purely for discussion purposes; the entire control run (1,156 years) is employed for the remainder of the analyses. During El Niño (La Niña) events, the Niño 3.4 region experiences positive (negative) SST anomalies that peak during boreal winter while the western Pacific experiences negative (positive) excursions (Trenberth, 1997). Strong El Niño and La Niña events yield SST anomalies that fall into the tails of the SSTA distribution (Figures 8b and 8c). An increase in the frequency and/or magnitude of strong ENSO events will increase the width of the SSTA distribution, and result in a larger standard deviation, a result previously illustrated using corals from the southwest Pacific (Lawman et al., 2020). This technique is ideally suited for data that has small uncertainty in the time domain or in the interpretation.

Longer-term changes in the amplitude and frequency of large SST anomalies can occur for decades or longer intervals (denoted here as decadal+ variability). For example, model years 100–120 (Figure 8a) have smaller amplitude SSTA compared to the frequent large-amplitude anomalies in model years 125–150. These changes occur in the absence of external forcing, as this is an unforced model simulation, and they likely result from complex interactions between ENSO and other internally driven modes of variability (Sun & Okumura, 2019; Wittenberg, 2009; Wittenberg et al., 2014). We quantify decadal+ changes in ENSO variability using the running standard deviation of climatology-removed monthly SSTA of 20-year windows averaged across the Niño 3.4 region ($\sigma_{Ni\tilde{3}.4-SSTA}$; Figure 8d) (Okumura et al., 2017). Larger $\sigma_{Ni\tilde{3}.4-SSTA}$ values indicate increased ENSO variability, whereas smaller $\sigma_{Ni\tilde{3}.4-SSTA}$ values indicate decreased ENSO variability during a time interval. The wide range of internal ENSO variability within the CESM-LME 850 control is reflected in the width of the $\sigma_{Ni\tilde{3}.4-SSTA}$ distribution (Figures 8e and 8f). We suggest that longer-term, decadal+ changes in ENSO variability, as reflected by $\sigma_{Ni\tilde{3}.4-SSTA}$ and the distribution of standard deviation values (Figure 8f), is a feasible target for coral-based paleoclimate reconstructions since this metric reduces the influence of uncertainties, especially temporal uncertainty.

3.3. Quantifying Changes in ENSO Variability Using Corals: Decadal+ With PSM

The coral PSM provides a tool to investigate how various uncertainties not only impact interannual variability locally, but also how the uncertainties broadly impact the ability of a pseudocoral to capture decadal+ changes ENSO variability. On interannual time scales, corals from circum-Pacific locations are influenced by ENSO, local variability, and how corals themselves records climate (section 1). Our coral PSM addresses some of these confounding influences by quantifying how analytical and calibration errors, variable growth rates, and age modeling assumptions modify input climate signals and impact interannual variance (section 2). The running standard deviation of climatology-removed anomalies is presented as an applicable metric in paleoclimate reconstructions for capturing temporal changes in interannual variability. This running standard deviation also provides a means to provide constraints on the range of internal variability (section 3.2). A running or windowed standard deviation is also advantageously poised to handle short (several decades or less) and/or discontinuous coral records, and has previously been employed for fossil

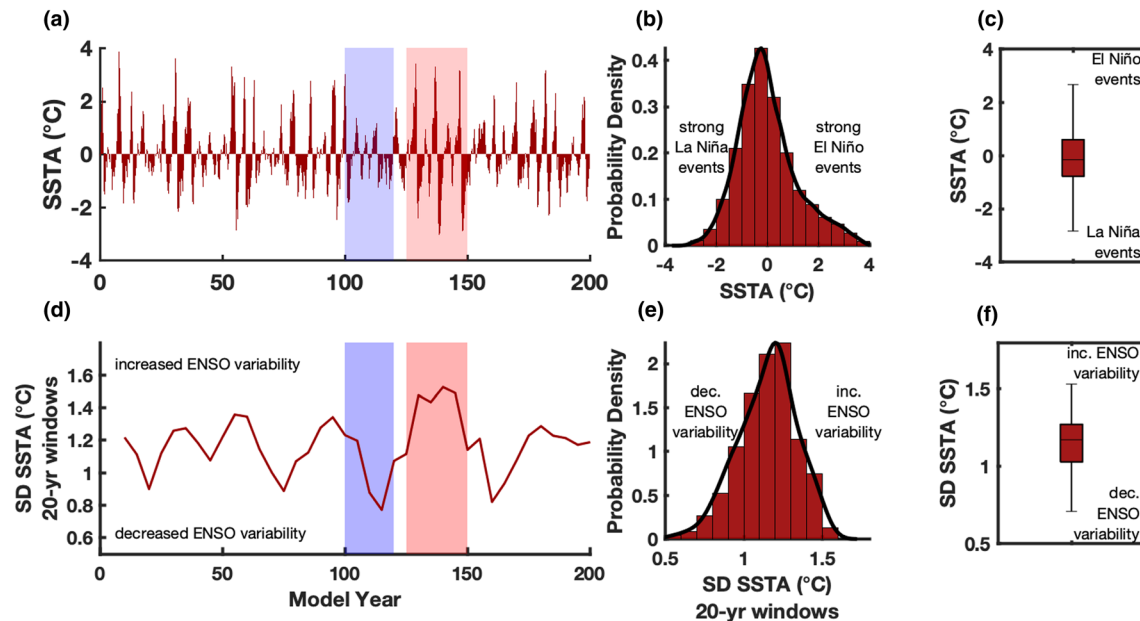


Figure 8. Quantifying changes in internal ENSO variability. (a) Monthly SSTA averaged across the Niño 3.4 region in the 850 control (200-year subset shown for clarity). Distribution of Niño 3.4 SSTA depicted as a histogram/PDF (b) and box plot (c) for the full-length control (1,156 years). (d) The 20-year running standard deviation of Niño 3.4 monthly SSTA ($\sigma_{\text{Niño3.4-SSTA}}$). Shaded portions in (a) and (d) highlight two intervals with more (red) and less (blue) internal ENSO variability. Distribution of $\sigma_{\text{Niño3.4-SSTA}}$ values depicted as a histogram/PDF (e) and box plot (f). Higher SD values indicate increased ENSO variability, whereas lower SD values indicate decreased variability. PDFs in (b) and (e) are based on a kernel density estimation method (Parzen, 1962). The lower and upper bounds of the boxes in (c) and (f) correspond to the 25th and 75th percentiles, and the center line indicates the median. The whiskers in (c) and (f) represent the $1.5 \times$ interquartile range (IQR). Outliers greater than $1.5 \times$ IQR are omitted for clarity. The running SD of monthly anomalies (f) is a metric for decadal+ changes in interannual variability.

coral records that are dated to cover snapshots of the last 7,000 years (the middle to late Holocene) (Cobb et al., 2013).

The 20-year running standard deviation of $\text{SST}_{\text{Sr/Ca}}$ and $\Delta\delta^{18}\text{O}_{\text{pseudocoral}}$ anomalies for Kiritimati and Vanuatu (Figure 9) demonstrate how the various PSM subcomponents impact interannual variance. This metric also encapsulates information about the range of simulated natural variability. As with Niño 3.4 monthly SSTA (Figure 8f), the median standard deviation value of the original environmental inputs (Figure 9, gray boxes) indicates the overall amplitude of interannual variance at a site, whereas the height of the box and whiskers indicate the range of internal variability. Kiritimati expectedly has a higher median standard deviation value and a larger spread compared to Vanuatu given that the site experiences larger interannual SST (Figure 6a) and $\delta^{18}\text{O}$ (Figure 6e) signals. Perturbing the original SST and $\Delta\delta^{18}\text{O}_{\text{pseudocoral}}$ time series at Kiritimati and Vanuatu with analytical and calibration errors (section 2.5.1) systematically increases interannual variance (Figure 9, light blue boxes) as quantified by the shift in the median standard deviation value compared to the original environmental inputs. Incorrect assumptions about the timing of the warmest and coolest month assignment in the age model (section 2.5.2) decreases interannual variance (Figure 9, teal boxes). We do not isolate the impact of variable growth rates as the algorithm generates a pseudodepth vector (section 4) that is not readily subset into 20-year windows. Instead, the original environmental input is perturbed with variable growth rates and then processed by the age model algorithm to generate multiple realizations (Figure 9, dark blue boxes). The combined influence of variable growth rates and the age model assumptions causes a systematic decrease in interannual variance at both sites.

Although each individual submodel of the PSM causes a systematic change in interannual variance at both Kiritimati and Vanuatu, the relative increase or decrease in the interannual signal (median standard deviation) for the full PSM, or the summation of the effects from the subcomponents, is site dependent. These site dependencies are revealed when expanding the pseudocoral network to the entire tropical Pacific (Figure 10). For similar reasons discussed in section 3.1, the interannual variance change is closely related to the ratio between the magnitude of the interannual signal and the amplitude of the annual cycle.

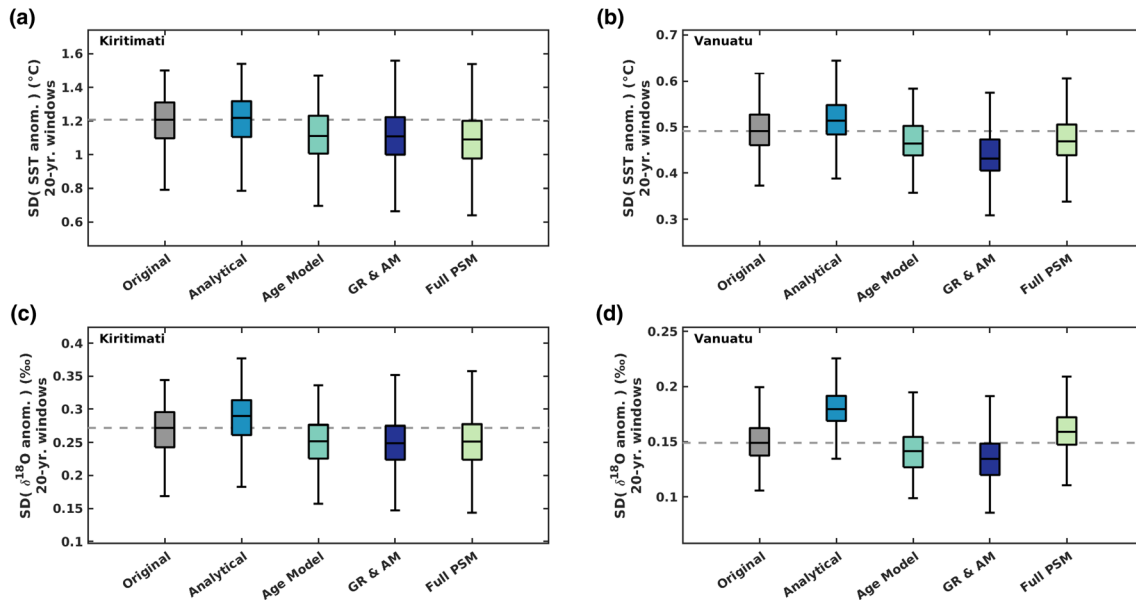


Figure 9. The impact of coral PSM uncertainties on interannual variance. Box plots showing the distribution of 20-year running standard deviation values for pseudocoral SST_{Sr/Ca} (a, c) and $\delta^{18}\text{O}$ (b, d) anomalies across all pseudocoral realizations for the Kiritimati (a, b) and Vanuatu (c, d) grid points. The growth rate and age model (GR & AM), analytical/calibration, and full PSM include the results for 1,000 realizations. The deterministic age modeled results are shown for 1 realization. The full PSM is determined by consecutively running the growth rate algorithm, applying analytical/calibration error, and then age modeling all 1,000 pseudocoral SST_{Sr/Ca} or $\delta^{18}\text{O}$ pseudocoral realizations. The lower and upper bounds of the boxes correspond to the 25th and 75th percentiles and the center line indicates the 50th percentile. The whiskers represent $1.5 \times \text{IQR}$. Outliers greater than $1.5 \times \text{IQR}$ are omitted for clarity. Dashed horizontal gray lines indicate the median SD for the original environmental inputs. The median 20-year running standard deviation of SST_{Sr/Ca} and $\delta^{18}\text{O}$ pseudocoral anomalies illustrates how the various PSM subcomponents systematically increase or decrease interannual variance. The length of the box and whiskers encapsulates information about the range of simulated internal variability.

We correlate Niño 3.4 SSTA with the pseudocoral realizations to demonstrate how corals from locations around the tropical Pacific record changes in ENSO and begin with the familiar month-to-month correlation calculation. The month-to-month correlation of local SST or SSS anomalies with Niño 3.4 SSTA is canonically used to demonstrate the ENSO sensitivity at a site. A consistent pattern of response over the 1,156-year-long control is the temperature relationship between the central/eastern and western tropical Pacific with monthly SSTA from the Niño 3.4 region (Figure 11a). For example, SSTA in the Niño 3.4 region and the central/eastern Pacific are in phase during ENSO events, meaning that when the Niño 3.4 region warms (cools), the central/eastern Pacific also warms (cools). During ENSO events SSTA in the Niño 3.4 region and

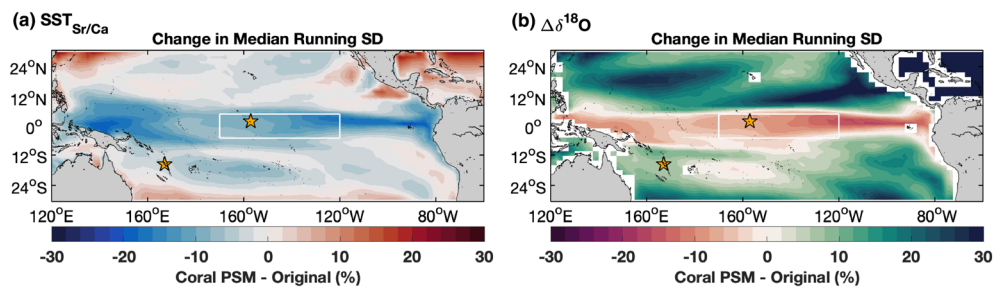


Figure 10. Changes in interannual variance for the full coral PSM. Percent difference in the median 20-year running standard deviation between pseudocoral SST_{Sr/Ca} (a) and $\delta^{18}\text{O}$ (b) anomalies perturbed with variable growth rates, analytical/calibration errors, and the age modeling algorithm, and the original, unperturbed environmental input ($n = 100$ realizations). Gold stars indicate select sites at Kiritimati and Vanuatu. The white box indicates the Niño 3.4 region. The percent change in standard deviation for the full coral PSM reveals the tradeoff between interannual variability and the amplitude of the annual cycle. The patterns displayed here are similar to those of Figure 6, indicating that the two variability metrics yield consistent results.

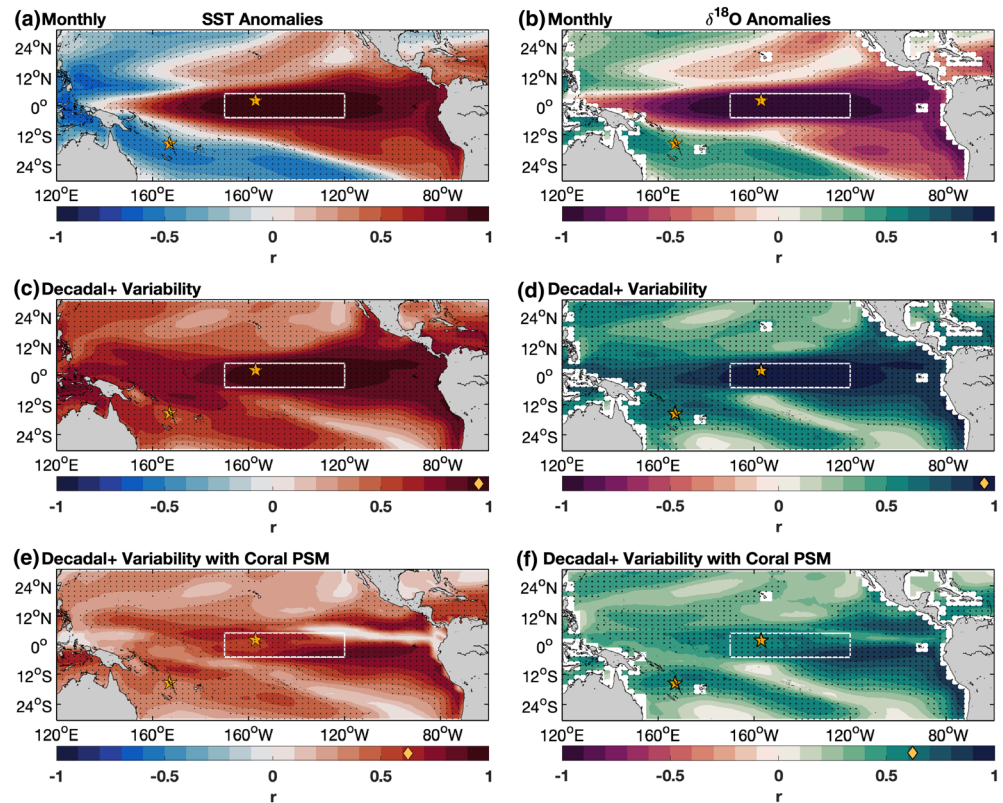


Figure 11. Correlation between Niño 3.4 SSTA and values at each grid point. Monthly Niño 3.4 correlated with monthly values for SSTA (a) and monthly values of forward modeled pseudocoral $\Delta\delta^{18}\text{O}_{\text{pseudocoral}}$ (b). The 20-year running SD of Niño 3.4 SSTA ($\sigma_{\text{Niño3.4-SSTA}}$) with the 20-year running SD of SSTA (c) and $\Delta\delta^{18}\text{O}_{\text{pseudocoral}}$ anomalies (d). The 20-year running SD of Niño 3.4 SSTA with the 20-year running standard deviation of SSTA (e) and $\Delta\delta^{18}\text{O}_{\text{pseudocoral}}$ anomalies (f) perturbed by the full coral PSM. Colormap in (e) and (f) is the median correlation coefficient for 100 full PSM realizations. The Niño 3.4 region is outlined by a white box (a–f). The correlation coefficient averaged across all grid points within the Niño 3.4 region (white box) is indicated with a gold diamond in (c)–(f). Colormaps provide the Pearson correlation coefficient (Pearson, 1920). $\Delta\delta^{18}\text{O}_{\text{pseudocoral}}$ is generated using the sensor model of Thompson et al. (2011) (section 2.3.1). Stippling indicates statistically significant correlations ($p < 0.01$) that accounts for autocorrelation in the time series (Dawdy & Matalas, 1964; Hu et al., 2017). Gold stars indicate select sites at Kiritimati and Vanuatu. Decadal+ changes in forward modeled interannual $\text{SST}_{\text{Sr/Ca}}$ and $\delta^{18}\text{O}$ variability are positively correlated with $\sigma_{\text{Niño3.4-SSTA}}$ across much of the tropical Pacific (e, f) even with the added uncertainties in our PSM, indicating that these processes do not obscure the target climate signal of decadal+ changes in ENSO variability.

the western Pacific are out of phase, such that when SSTA are warm in the Niño 3.4 region SSTA in the western Pacific are cool, and vice versa. Forward modeled monthly $\Delta\delta^{18}\text{O}_{\text{pseudocoral}}$, a function of SST and SSS, also covaries with Niño 3.4 SSTA (Figure 11b) with nearly the same pattern of response as SSTA (Figure 11a). For example, during El Niño events the central and eastern Pacific experience negative $\Delta\delta^{18}\text{O}_{\text{pseudocoral}}$ anomalies indicating the combined impact of warmer and/or fresher conditions, while the western Pacific experiences positive $\Delta\delta^{18}\text{O}_{\text{pseudocoral}}$ excursions indicative of cooler and/or more saline conditions (Fairbanks et al., 1997). As previously discussed, the month-to-month correlation with Niño 3.4 SSTA is more applicable for observations or model output with no uncertainty in the time domain. Some of the uncertainties in coral proxy data can be circumvented by instead shifting the focus to the ability of a coral to capture ENSO variability on decadal+ time scales (section 3.2).

Unlike the month-to-month maps, Niño 3.4 SSTA and the running standard deviation of $\text{SST}_{\text{Sr/Ca}}$ and $\Delta\delta^{18}\text{O}_{\text{pseudocoral}}$ anomalies on decadal+ time scales are positively correlated across much of the tropical Pacific (Figures 11c and 11d). The boomerang-shaped monthly SSTA correlation pattern that distinguishes the western Pacific from the central/eastern Pacific (Figure 11a) essentially disappears when examining how different regions of the Pacific track decadal+ changes in ENSO variability. The nodal structure

(where the red color changes to blue in the month-to-month calculation), where the correlation is essentially zero (Figures 11a and 11b), is still apparent in decadal+. In the decadal+ calculation of ENSO variability, a significant positive correlation coefficient between $\sigma_{\text{Niño3.4-SSTA}}$ and the running standard deviation of monthly SST (Figure 11c) or $\Delta\delta^{18}\text{O}_{\text{pseudocoral}}$ (Figure 11d) anomalies indicates that when ENSO variability increases or decreases in the Niño 3.4 region, interannual variability at a given location tends to pace with those changes. The correlation with $\sigma_{\text{Niño3.4-SSTA}}$ for the pseudocorals perturbed by the full coral PSM are expectedly smaller than the original PSM inputs, but importantly, the temporal relationship with changes in SST variability in the Niño 3.4 region is broadly preserved for both pseudocoral $\text{SST}_{\text{Sr/Ca}}$ (Figure 11e) and $\Delta\delta^{18}\text{O}_{\text{pseudocoral}}$ (Figure 11f). Despite all of the calculated coral uncertainties, the correlation with decadal+ changes in ENSO remains statistically significant at many circum-Pacific locations, particularly those near coral atolls (Figures 11e and 11f). This highlights the strength of corals in their ability to capture decadal+ changes in ENSO variability.

4. Conclusions

The coral PSM presented here advances our knowledge of how corals modify interannual climate signals and how they record changes in ENSO variability via the decadal+ calculation. This study builds upon previous work by adding new archive and observation submodels to the full PSM framework in order to quantitatively estimate the impact of various nonclimatic processes on interannual variance in the final coral time series. Constraining such information is crucial given that quantitative estimates of interannual variance is one of the primary applications of coral paleoclimatology. Our process-based coral PSM explicitly incorporates an archive-based model (variable growth rates) as well as age modeling assumptions that are used when generating a coral geochemical time series. This study applies the new PSM framework to the CESM LME 850 control run, which serves as the environmental input. The long control run allows us to include the impact of a wide range of internal variability in our analyses, which is not possible using the short instrumental record. Although we note that the PSM is equally equipped to handle observational data or output from other climate models. Our tools and algorithms are publicly available to the broader community to facilitate the comparison of coral geochemical data and observational data or climate model output, as well as facilitate the reproducibility of our results, via a GitHub repository (<https://github.com/lawmana/coralPSM>).

Our results characterize and document the ability of pseudocorals to capture decadal and longer, which we call decadal+, changes in ENSO variability. Coral proxy records of past ENSO variability come from a suite of sites spanning the western, central, and eastern tropical Pacific, all of which have varying signal-to-noise ratios with respect to ENSO. In some regions of the tropical Pacific, the combination of different uncertainties can increase or decrease interannual $\text{SST}_{\text{Sr/Ca}}$ and $\delta^{18}\text{O}$ variance by 10–30% (Figures 7 and 10). We identify four broad conclusions from these analyses:

1. Analytical and calibration errors systematically increase interannual variance.
2. Seasonal chronological uncertainties associated with transforming coral geochemical data from the depth to the time domain act to decrease interannual variability.
3. Variable growth rates in conjunction with age modeling assumptions decrease interannual variance.
4. The change in interannual variance at a given location is related to the relative magnitudes of the interannual ENSO signal and the amplitude of the annual cycle.

Given that different processes exert sizable impacts on interannual variance, it is therefore most appropriate to compare coral geochemical data with instrumental observations or climate model output processed through the new coral PSM. Despite the three uncertainties investigated in this study, the temporal relationship with changes in SST variability in the Niño 3.4 region is preserved for both pseudocoral $\text{SST}_{\text{Sr/Ca}}$ (Figure 11e) and $\Delta\delta^{18}\text{O}_{\text{pseudocoral}}$ (Figure 11f). Importantly, decadal+ changes in forward-modeled interannual $\text{SST}_{\text{Sr/Ca}}$ and $\delta^{18}\text{O}$ variability are positively correlated with $\sigma_{\text{Niño3.4-SSTA}}$ across much of the tropical Pacific. Despite all of the added uncertainties in our PSM, at many locations these processes do not obscure the target climate signal of decadal and longer changes in ENSO variability and yield statistically significant correlations with $\sigma_{\text{Niño3.4-SSTA}}$. This increases confidence that despite these major sources of uncertainties investigated herein, coral geochemical records from a suite of sites across the tropical Pacific are useful tools to reconstruct changes in ENSO variability back in time.

Quantifying the range of ENSO variability experienced during different background climate states in the past is critical, as this data can help constrain models that provide projections of how ENSO variability may change in the future with anthropogenic warming. Paleoclimate reconstructions serve as important out-of-sample tests of ENSO variability, and climate models that are able to simulate past changes in ENSO may be better equipped to project how ENSO will change in the future. Proxy system modeling studies, such as this one that incorporates information from both models and proxy records, are necessary to compare model estimates of paleo-ENSO variability with coral geochemical data. By putting climate model output and proxy data on a level playing field, we can reconcile the agreement between climate models and proxy-inferred responses and take an important step toward predicting how ENSO will respond to future radiative forcing.

Data Availability Statement

The climate model output used in this study is from the Community Earth System Model Last Millennium Ensemble (CESM-LME) 850 control simulation (Otto-Bliesner et al., 2016). The output is publicly archived on the Earth System Grid as single variable time series (<https://www.earthsystemgrid.org/>). The monthly atmospheric components are available at this site (https://www.earthsystemgrid.org/dataset/ucar.cgd.cesm4.CESM_CAM5_LME.atm.proc.monthly_ave.html). The monthly oceanic components are available at this site (https://www.earthsystemgrid.org/dataset/ucar.cgd.cesm4.CESM_CAM5_LME.ocn.proc.monthly_ave.html). The MATLAB® codes for the coral PSM algorithms that contributed to the analysis and results in this study are publicly available on the GitHub repository for the lead author (<https://github.com/lawmana/coralPSM>). We also acknowledge the use of the Climate Data Toolbox (CDT) for MATLAB® (Greene et al., 2019). The CDT is publicly available on GitHub (<https://github.com/chadagreene/CDT>). We also acknowledge the use of the cmocean: colormaps for oceanography toolbox (Thyng et al., 2016) that is available on the MathWorks® File Exchange (<https://www.mathworks.com/matlabcentral/fileexchange/57773-cmocean-perceptually-uniform-colormaps>). We also acknowledge the use of M_Map: A Mapping Package for MATLAB® available at this site (<https://www.eoas.ubc.ca/~rich/map.html>).

Conflict of Interest

The authors declare no competing financial interests.

Acknowledgments

This research was supported by NSF grant #1805874 under the Paleoclimate Perspectives on Climate Change (P2C2) competition (to J.W.P.) and the National Science Foundation Graduate Research Fellowship Program (to A.E.L.). We thank Tim Shanahan and Rowan Martindale for their feedback on manuscript. We also thank Anthony Krupa for helping A.E.L. measure the annual coral growth rates used to develop the parameters for the growth rate AR(2) model. We thank the members of the PAGES Data Assimilation and Proxy System Modeling (DAPS) community for their feedback at the May 2019 working group meeting.

References

- Alibert, C., & McCulloch, M. T. (1997). Strontium/calcium ratios in modern *Porites* corals from the great barrier reef as a proxy for sea surface temperature: Calibration of the thermometer and monitoring of ENSO. *Paleoceanography*, 12(3), 345–363. <https://doi.org/10.1029/97PA00318>
- Ault, T. R., Cole, J. E., Evans, M. N., Barnett, H., Abram, N. J., Tudhope, A. W., & Linsley, B. K. (2009). Intensified decadal variability in tropical climate during the late 19th century. *Geophysical Research Letters*, 36, 2209. <https://doi.org/10.1029/2008GL036924>
- Beck, J. W., Edwards, R. L., Ito, E., Taylor, F. W., Recy, J., Rougerie, F., et al. (1992). Sea-surface temperature from coral skeletal strontium/calcium ratios. *Science*, 257(5070), 644–647. <https://doi.org/10.1126/science.257.5070.644>
- Bellenger, H., Guilyardi, E., Leloup, J., Lengaigne, M., & Vialard, J. (2014). ENSO representation in climate models: From CMIP3 to CMIP5. *Climate Dynamics*, 42(7–8), 1999–2018. <https://doi.org/10.1007/s00382-013-1783-z>
- Bjerknes, J. (1969). Atmospheric teleconnections from the equatorial pacific. *Monthly Weather Review*, 97(3), 163–172. [https://doi.org/10.1175/1520-0493\(1969\)097%3C0163:ATFTEP%3E2.3.CO;2](https://doi.org/10.1175/1520-0493(1969)097%3C0163:ATFTEP%3E2.3.CO;2)
- Brown, J., Tudhope, A. W., Collins, M., & McGregor, H. V. (2008). Mid-Holocene ENSO: Issues in quantitative model-proxy data comparisons. *Paleoceanography*, 23, PA3202. <https://doi.org/10.1029/2007PA001512>
- Cai, W., Borlace, S., Lengaigne, M., van Rensch, P., Collins, M., Vecchi, G., et al. (2014). Increasing frequency of extreme El Niño events due to greenhouse warming. *Nature Climate Change*, 4(2), 111–116. <https://doi.org/10.1038/nclimate2100>
- Cai, W., Wang, G., Santoso, A., McPhaden, M. J., Wu, L., Jin, F. F., et al. (2015). Increased frequency of extreme La Niña events under greenhouse warming. *Nature Climate Change*, 5(2), 132–137. <https://doi.org/10.1038/nclimate2492>
- Cheng, H., Lawrence Edwards, R., Shen, C. C., Polyak, V. J., Asmerom, Y., Woodhead, J., et al. (2013). Improvements in ²³⁰Th dating, ²³⁰Th and ²³⁴U half-life values, and U–Th isotopic measurements by multi-collector inductively coupled plasma mass spectrometry. *Earth and Planetary Science Letters*, 371–372(C), 82–91. <https://doi.org/10.1016/j.epsl.2013.04.006>
- Chung, E.-S., Timmermann, A., Soden, B. J., Ha, K.-J., Shi, L., & John, V. O. (2019). Reconciling opposing Walker circulation trends in observations and model projections. *Nature Climate Change*, 9(5), 405–412. <https://doi.org/10.1038/s41558-019-0446-4>
- Cobb, K. M., Westphal, N., Sayani, H. R., Watson, J. T., Di Lorenzo, E., Cheng, H., et al. (2013). Highly variable El Niño–Southern Oscillation throughout the Holocene. *Science*, 339(6115), 67–70. <https://doi.org/10.1126/science.1228246>
- Cole, J. E., Fairbanks, R. G., & Shen, G. T. (1993). Recent variability in the Southern Oscillation: Isotopic results from a Tarawa Atoll coral. *Science*, 260(5115), 1790–1793. <https://doi.org/10.1126/science.260.5115.1790>
- Collins, M., An, S. I., Cai, W., Ganachaud, A., Guilyardi, E., Jin, F. F., et al. (2010). The impact of global warming on the tropical Pacific Ocean and El Niño. *Nature Geoscience*, 3(6), 391–397. <https://doi.org/10.1038/ngeo868>

- Collins, M., Knutti, R., Arblaster, J., Dufresne, J., Fichet, T., Friedlingstein, P., et al. (2013). Long-term climate change: Projections, commitments and irreversibility. In *Climate Change 2013: The Physical Science Basis. Contribution of Working Group I to the Fifth Assessment Report of the Intergovernmental Panel on Climate Change* (pp. 1–108). Cambridge, UK, and New York, NY: Cambridge University Press.
- Comboul, M., Emile-Geay, J., Evans, M. N., Mirnateghi, N., Cobb, K. M., & Thompson, D. M. (2014). A probabilistic model of chronological errors in layer-counted climate proxies: Applications to annually banded coral archives. *Climate of the Past*, 10(2), 825–841. <https://doi.org/10.5194/cp-10-825-2014>
- Conroy, J. L., Thompson, D. M., Cobb, K. M., Noone, D., Rea, S., & LeGrande, A. N. (2017). Spatiotemporal variability in the $\delta^{18}\text{O}$ -salinity relationship of seawater across the tropical Pacific Ocean. *Paleoceanography*, 32, 484–497. <https://doi.org/10.1002/2016PA003073>
- Corrège, T. (2006). Sea surface temperature and salinity reconstruction from coral geochemical tracers. *Palaeogeography, Palaeoclimatology, Palaeoecology*, 232(2–4), 408–428. <https://doi.org/10.1016/j.palaeo.2005.10.014>
- Dawdy, D., & Matalas, N. (1964). Statistical and probability analysis of hydrologic data, part III: Analysis of variance, covariance and time series. In V. T. Chow (Ed.), *Handbook of Applied Hydrology: A Compendium of Water-Resources Technology*. New York, NY: McGraw-Hill.
- Dee, S., Emile-Geay, J., Evans, M. N., Allam, A., Steig, E. J., & Thompson, D. M. (2015). PRYSM: An open-source framework for PROXY system modeling, with applications to oxygen-isotope systems. *Journal of Advances in Modeling Earth Systems*, 7, 1220–1247. <https://doi.org/10.1002/2015MS000447>
- Dee, S. G., Russell, J. M., Morrill, C., Chen, Z., & Neary, A. (2018). PRYSM v2.0: A proxy system model for lacustrine archives. *Paleoceanography and Paleoclimatology*, 33, 1250–1269. <https://doi.org/10.1029/2018PA003413>
- DeLong, K. L., Quinn, T. M., Taylor, F. W., Lin, K., & Shen, C.-C. (2012). Sea surface temperature variability in the southwest tropical Pacific since AD 1649. *Nature Climate Change*, 2(11), 799–804. <https://doi.org/10.1038/nclimate1583>
- DeLong, K. L., Quinn, T. M., Taylor, F. W., Shen, C.-C., & Lin, K. (2013). Improving coral-base paleoclimate reconstructions by replicating 350 years of coral Sr/Ca variations. *Palaeogeography, Palaeoclimatology, Palaeoecology*, 373(C), 6–24. <https://doi.org/10.1016/j.palaeo.2012.08.019>
- Deser, C., Alexander, M. A., Xie, S.-P., & Phillips, A. S. (2010). Sea surface temperature variability: Patterns and mechanisms. *Annual Review of Marine Science*, 2(1), 115–143. <https://doi.org/10.1146/annurev-marine-120408-151453>
- Deser, C., Phillips, A. S., Tomas, R. A., Okumura, Y., Alexander, M. A., Capotondi, A., et al. (2012). ENSO and Pacific decadal variability in the Community Climate System Model version 4. *Journal of Climate*, 25(8), 2622–2651. <https://doi.org/10.1175/JCLI-D-11-00301.1>
- DiNezio, P. N., Deser, C., Karspeck, A., Yeager, S., Okumura, Y., Danabasoglu, G., et al. (2017). A 2 year forecast for a 60–80% chance of La Niña in 2017–2018. *Geophysical Research Letters*, 44, 11,624–11,635. <https://doi.org/10.1002/2017GL074904>
- DiNezio, P. N., Vecchi, G. A., & Clement, A. C. (2013). Detectability of changes in the Walker circulation in response to global warming. *Journal of Climate*, 26(12), 4038–4048. <https://doi.org/10.1175/JCLI-D-12-00531.1>
- Emile-Geay, J., Cobb, K. M., Carré, M., Braconnot, P., Leloup, J., Zhou, Y., et al. (2016). Links between tropical Pacific seasonal, interannual and orbital variability during the Holocene. *Nature Geoscience*, 9(2), 168–173. <https://doi.org/10.1038/ngeo2608>
- Emile-Geay, J., Cobb, K. M., Mann, M. E., & Wittenberg, A. T. (2013a). Estimating central equatorial Pacific SST variability over the past millennium. Part I: Methodology and validation. *Journal of Climate*, 26(7), 2302–2328. <https://doi.org/10.1175/JCLI-D-11-00510.1>
- Emile-Geay, J., Cobb, K. M., Mann, M. E., & Wittenberg, A. T. (2013b). Estimating central equatorial Pacific SST variability over the past millennium. Part II: Reconstructions and implications. *Journal of Climate*, 26(7), 2329–2352. <https://doi.org/10.1175/JCLI-D-11-00511.1>
- Epstein, S., Buchsbaum, R., Lowenstam, H. A., & Urey, H. C. (1953). Revised carbonate-water isotopic temperature scale. *Geological Society of America Bulletin*, 64(11), 1315–1326. [https://doi.org/10.1130/0016-7606\(1953\)64\[1315:RCITS\]2.0.CO;2](https://doi.org/10.1130/0016-7606(1953)64[1315:RCITS]2.0.CO;2)
- Evans, M. N. (2007). Toward forward modeling for paleoclimatic proxy signal calibration: A case study with oxygen isotopic composition of tropical woods. *Geochemistry, Geophysics, Geosystems*, 8, Q07008. <https://doi.org/10.1029/2006GC001406>
- Evans, M. N., Kaplan, A., & Cane, M. A. (2000). Intercomparison of coral oxygen isotope data and historical sea surface temperature (SST): Potential for coral-based SST field reconstructions. *Paleoceanography*, 15(5), 551–563. <https://doi.org/10.1029/2000PA000498>
- Evans, M. N., Tolwinski-Ward, S. E., Thompson, D. M., & Anchukaitis, K. J. (2013). Applications of proxy system modeling in high resolution paleoclimatology. *Quaternary Science Reviews*, 76(c), 16–28. <https://doi.org/10.1016/j.quascirev.2013.05.024>
- Fairbanks, R. G., Evans, M. N., Rubenstone, J. L., Mortlock, R. A., Broad, K., Moore, M. D., & Charles, C. D. (1997). Evaluating climate indices and their geochemical proxies measured in corals. *Coral Reefs*, 16(5), S93–S100. <https://doi.org/10.1007/s003380050245>
- Friedman, I., & O'Neil, J. R. (1977). Compilation of stable isotope fractionation factors of geochemical interest. M. Fleischer (Ed.), *Data of geochemistry* (Vol. 440, 6th). U.S. Government Printing Office.
- Fritsch, F. N., & R. C. S. J. O. N. Analysis (1980). Monotone piecewise cubic interpolation. *SIAM*, 17(2), 238–246. <https://doi.org/10.1137/0717021>
- Gagan, M. K., Ayliffe, L. K., Beck, J. W., Cole, J. E., Druffel, E., Dunbar, R. B., & Schrag, D. P. (2000). New views of tropical paleoclimates from corals. *Quaternary Science Reviews*, 19(1–5), 45–64. [https://doi.org/10.1016/S0277-3791\(99\)00054-2](https://doi.org/10.1016/S0277-3791(99)00054-2)
- Gagan, M. K., Ayliffe, L. K., Hopley, D., Cali, J. A., Mortimer, G. E., Chappell, J., et al. (1998). Temperature and Surface-Ocean water balance of the mid-Holocene tropical Western Pacific. *Science*, 279(5353), 1014–1018. <https://doi.org/10.1126/science.279.5353.1014>
- Gorman, M. K., Quinn, T. M., Taylor, F. W., Partin, J. W., Cabioch, G., Austin, J. A. Jr., et al. (2012). A coral-based reconstruction of sea surface salinity at Sabine Bank, Vanuatu from 1842 to 2007 CE. *Paleoceanography*, 27, PA3226. <https://doi.org/10.1029/2012PA002302>
- Greene, C. A., Thirumalai, K., Kearney, K. A., Delgado, J. M., Schwanghart, W., Wolfenbarger, N. S., et al. (2019). The climate data toolbox for MATLAB. *Geochemistry, Geophysics, Geosystems*, 15, 379–3781. <https://doi.org/10.1029/2019GC008392>
- Grotoli, A. G., & Eakin, C. M. (2007). A review of modern coral $\delta^{18}\text{O}$ and $\Delta^{14}\text{C}$ proxy records. *Earth Science Reviews*, 81(1–2), 67–91. <https://doi.org/10.1016/j.earscirev.2006.10.001>
- Hathorne, E. C., Gagnon, A., Felis, T., Adkins, J., Asami, R., Boer, W., et al. (2013). Interlaboratory study for coral Sr/Ca and other element/Ca ratio measurements. *Geochemistry, Geophysics, Geosystems*, 14, 3730–3750. <https://doi.org/10.1002/ggge.20230>
- Hereid, K. A., Quinn, T. M., & Okumura, Y. M. (2013). Assessing spatial variability in El Niño–Southern Oscillation event detection skill using coral geochemistry. *Paleoceanography*, 28, 14–23. <https://doi.org/10.1029/2012PA002352>
- Hereid, K. A., Quinn, T. M., Taylor, F. W., Shen, C. C., Lawrence Edwards, R., & Cheng, H. (2013). Coral record of reduced El Niño activity in the early 15th to middle 17th centuries. *Geology*, 41(1), 51–54. <https://doi.org/10.1130/G33510.1>
- Herron, M. M., & Langway, C. C. (2017). Firn densification: An empirical model. *Journal of Glaciology*, 25(93), 373–385. <https://doi.org/10.3189/S0022143000015239>

- Hu, J., Emile-Geay, J., & Partin, J. (2017). Correlation-based interpretations of paleoclimate data—Where statistics meet past climates. *Earth and Planetary Science Letters*, 459, 362–371. <https://doi.org/10.1016/j.epsl.2016.11.04>
- Hurrell, J. W., Holland, M. M., Gent, P. R., Ghan, S., Kay, J. E., Kushner, P. J., et al. (2013). The Community Earth System Model: A framework for collaborative research. *Bulletin of the American Meteorological Society*, 94(9), 1339–1360. <https://doi.org/10.1175/BAMS-D-12-00121.1>
- Jimenez, G., Cole, J. E., Thompson, D. M., & Tudhope, A. W. (2018). Northern Galápagos corals reveal twentieth century warming in the eastern tropical Pacific. *Geophysical Research Letters*, 45, 1981–1988. <https://doi.org/10.1002/2017GL075323>
- Johnsen, S. J., Clausen, H. B., Cuffey, K. M., Hoffmann, G., & Creyts, T. T. (2000). Diffusion of stable isotopes in polar firn and ice: The isotope effect in firn diffusion. *Physics of Ice Core Records*, 159, 121–140. <https://doi.org/10.7916/D8KW5D4X>
- Kilbourne, K. H., Quinn, T. M., Taylor, F. W., Delcroix, T., & Gouriou, Y. (2004). El Niño-southern oscillation-related salinity variations recorded in the skeletal geochemistry of a *Porites* coral from Espiritu Santo, Vanuatu. *Paleoceanography*, 19, PA4002. <https://doi.org/10.1029/2004PA001033>
- Lawman, A. E., Quinn, T. M., Partin, J. W., Thirumalai, K., Taylor, F. W., Wu, C. C., et al. (2020). A century of reduced ENSO variability during the medieval climate anomaly. *Paleoceanography and Paleoclimatology*, 35, e2019PA003742. <https://doi.org/10.1029/2019PA003742>
- LeGrande, A. N., & Schmidt, G. A. (2006). Global gridded data set of the oxygen isotopic composition in seawater. *Geophysical Research Letters*, 33, L12604. <https://doi.org/10.1029/2006GL026011>
- Linsley, B. K., Kaplan, A., & Gouriou, Y. (2006). Tracking the extent of the South Pacific convergence zone since the early 1600s. *Geochemistry, Geophysics, Geosystems*, 7, Q05003. <https://doi.org/10.1029/2005GC001115>
- Lough, J. M. (2004). A strategy to improve the contribution of coral data to high-resolution paleoclimatology. *Palaeogeography, Palaeoclimatology, Palaeoecology*, 204(1–2), 115–143. [https://doi.org/10.1016/S0031-0182\(03\)00727-2](https://doi.org/10.1016/S0031-0182(03)00727-2)
- Lough, J. M. (2010). Climate records from corals. *WIREs Climate Change*, 1(3), 318–331. <https://doi.org/10.1002/wcc.39>
- Okumura, Y. M., Sun, T., & Wu, X. (2017). Asymmetric modulation of El Niño and La Niña and the linkage to tropical Pacific decadal variability. *Journal of Climate*, 30(12), 4705–4733. <https://doi.org/10.1175/JCLI-D-16-0680.1>
- Otto-Bliesner, B. L., Brady, E. C., Fasullo, J., Jahn, A., Landrum, L., Stevenson, S., et al. (2016). Climate variability and change since 850 CE: An ensemble approach with the Community Earth System Model. *Bulletin of the American Meteorological Society*, 97(5), 735–754. <https://doi.org/10.1175/BAMS-D-14-00233.1>
- Partin, J. W., Quinn, T. M., Shen, C. C., Emile-Geay, J., Taylor, F. W., Maupin, C. R., et al. (2013). Multidecadal rainfall variability in South Pacific convergence zone as revealed by stalagmite geochemistry. *Geology*, 41(11), 1143–1146. <https://doi.org/10.1130/G34718.1>
- Parzen, E. (1962). On estimation of a probability density function and mode. *Annals of Mathematical Statistics*, 33(3), 1065–1076. <https://doi.org/10.1214/aoms/1177704472>
- Pearson, K. (1920). Notes on the history of correlation. *Biometrika*, 13(1), 25. <https://doi.org/10.2307/2331722>
- Quinn, T. M., & Sampson, D. E. (2002). A multiproxy approach to reconstructing sea surface conditions using coral skeleton geochemistry. *Paleoceanography*, 17(4), 1062. <https://doi.org/10.1029/2000PA000528>
- Ren, L., Linsley, B. K., Wellington, G. M., Schrag, D. P., & Hoegh-guldberg, O. (2003). Deconvolving the $\delta^{18}\text{O}$ seawater component from subseasonal coral $\delta^{18}\text{O}$ and Sr/Ca at Rarotonga in the southwestern subtropical Pacific for the period 1726 to 1997. *Geochimica et Cosmochimica Acta*, 67(9), 1609–1621. [https://doi.org/10.1016/S0016-7037\(02\)00917-1](https://doi.org/10.1016/S0016-7037(02)00917-1)
- Roden, J. S., Lin, G., & Ehleringer, J. R. (2000). A mechanistic model for interpretation of hydrogen and oxygen isotope ratios in tree-ring cellulose. *Geochimica et Cosmochimica Acta*, 64(1), 21–35. [https://doi.org/10.1016/S0016-7037\(99\)00195-7](https://doi.org/10.1016/S0016-7037(99)00195-7)
- Ropelewski, C. F., & Halpert, M. S. (1987). Global and regional scale precipitation patterns associated with the El Niño/Southern Oscillation. *Monthly Weather Review*, 115(8), 1606–1626. [https://doi.org/10.1175/1520-0493\(1987\)115%3C1606:GARSPP%3E2.0.CO;2](https://doi.org/10.1175/1520-0493(1987)115%3C1606:GARSPP%3E2.0.CO;2)
- Russon, T., Tudhope, A. W., & Research, M. C. G. (2015). Inferring changes in ENSO amplitude from the variance of proxy records. *Geophysical Research Letters*, 42, 1197–1204. [https://doi.org/10.1002/\(ISSN\)1944-8007](https://doi.org/10.1002/(ISSN)1944-8007)
- Sayani, H. R., Cobb, K. M., DeLong, K., Hitt, N. T., & Druffel, E. R. M. (2019). Intercolony $\delta^{18}\text{O}$ and Sr/Ca variability among *Porites* spp. corals at Palmyra atoll: Towards more robust coral-based estimates of climate. *Geochemistry, Geophysics, Geosystems*, 20, 5270–5284. <https://doi.org/10.1029/2019GC008420>
- Schmidt, G. A., Annan, J. D., Bartlein, P. J., Cook, B. I., Guiliardi, E., Hargreaves, J. C., et al. (2014). Using palaeo-climate comparisons to constrain future projections in CMIP5. *Climate of the Past*, 10(1), 221–250. <https://doi.org/10.5194/cp-10-221-2014>
- Schrag, D. P. (1999). Rapid analysis of high-precision Sr/Ca ratios in corals and other marine carbonates. *Paleoceanography*, 14(2), 97–102. <https://doi.org/10.1029/1998PA000025>
- Shen, C.-C., Wu, C. C., Cheng, H., Lawrence Edwards, R., Hsieh, Y. T., Gallet, S., et al. (2012). High-precision and high-resolution carbonate ^{230}Th dating by MC-ICP-MS with SEM protocols. *Geochimica et Cosmochimica Acta*, 99(C), 71–86. <https://doi.org/10.1016/j.gca.2012.09.018>
- Smith, S. V., Buddemeier, R. W., Redalje, R. C., & Houck, J. E. (1979). Strontium-calcium thermometry in coral skeletons. *Science*, 204(4391), 404–407. <https://doi.org/10.1126/science.204.4391.404>
- Stevenson, S., Fox-Kemper, B., Jochum, M., Rajagopalan, B., & Yeager, S. G. (2010). ENSO model validation using wavelet probability analysis. *Journal of Climate*, 23(20), 5540–5547. <https://doi.org/10.1175/2010JCLI3609.1>
- Stevenson, S., McGregor, H. V., Phipps, S. J., & Fox-Kemper, B. (2013). Quantifying errors in coral-based ENSO estimates: Toward improved forward modeling of $\delta^{18}\text{O}$. *Paleoceanography*, 28, 633–649. <https://doi.org/10.1002/palo.20059>
- Stevenson, S., Powell, B. S., Merrifield, M. A., Cobb, K. M., Nusbaumer, J., & Noone, D. (2015). Characterizing seawater oxygen isotopic variability in a regional ocean modeling framework: Implications for coral proxy records. *Paleoceanography*, 30, 1573–1593. <https://doi.org/10.1002/2015PA002824>
- Sun, T., & Okumura, Y. M. (2019). Role of stochastic atmospheric forcing from the south and North Pacific in tropical Pacific decadal variability. *Journal of Climate*, 32(13), 4013–4038. <https://doi.org/10.1175/JCLI-D-18-0536.1>
- Thompson, D. M., Ault, T. R., Evans, M. N., Cole, J. E., & Emile-Geay, J. (2011). Comparison of observed and simulated tropical climate trends using a forward model of coral $\delta^{18}\text{O}$. *Geophysical Research Letters*, 38, L14706. <https://doi.org/10.1029/2011GL048224>
- Thyng, K., Greene, C., Hetland, R., Zimmerle, H., & DiMarco, S. (2016). True colors of oceanography: Guidelines for effective and accurate colormap selection. *Oceanography*, 29(3), 9–13. <https://doi.org/10.5670/oceanog.2016.66>
- Trenberth, K. E. (1997). The definition of El Niño. *Bulletin of the American Meteorological Society*, 78(12), 2771–2777. [https://doi.org/10.1175/1520-0477\(1997\)078%3C2771:TDOENO%3E2.0.CO;2](https://doi.org/10.1175/1520-0477(1997)078%3C2771:TDOENO%3E2.0.CO;2)
- Trenberth, K. E., & Hoar, T. J. (1996). The 1990–1995 El Niño-Southern Oscillation event: Longest on record. *Geophysical Research Letters*, 23(1), 57–60. <https://doi.org/10.1029/95GL03602>

- Wang, B., Luo, X., Yang, Y.-M., Sun, W., Cane, M. A., Cai, W., et al. (2019). Historical change of El Niño properties sheds light on future changes of extreme El Niño. *Proceedings of the National Academy of Sciences of the United States of America*, 116(45), 22512–22517. <https://doi.org/10.1073/pnas.1911130116>
- Weber, J. N. (1973). Incorporation of strontium into reef coral skeletal carbonate. *Geochimica et Cosmochimica Acta*, 37(9), 2173–2190. [https://doi.org/10.1016/0016-7037\(73\)90015-X](https://doi.org/10.1016/0016-7037(73)90015-X)
- Weber, J. N., & Woodhead, P. M. J. (1972). Temperature dependence of oxygen-18 concentration in reef coral carbonates. *Journal of Geophysical Research, Oceans*, 77(3), 463–473. <https://doi.org/10.1029/JC077i003p00463>
- Wittenberg, A. T. (2009). Are historical records sufficient to constrain ENSO simulations? *Geophysical Research Letters*, 36, L12702. <https://doi.org/10.1029/2009GL038710>
- Wittenberg, A. T., Rosati, A., Delworth, T. L., Vecchi, G. A., & Zeng, F. (2014). ENSO modulation: Is it decadal predictable? *Journal of Climate*, 27(7), 2667–2681. <https://doi.org/10.1175/JCLI-D-13-00577.1>
- Wong, C. I., & Breecker, D. O. (2015). Advancements in the use of speleothems as climate archives. *Quaternary Science Reviews*, 127, 1–18. <https://doi.org/10.1016/j.quascirev.2015.07.019>
- Wu, X., Okumura, Y. M., & DiNezio, P. N. (2019). What controls the duration of El Niño and La Niña events? *Journal of Climate*, 32(18), 5941–5965. <https://doi.org/10.1175/JCLI-D-18-0681.1>